Nanoscale Advances

ROYAL SOCIETY OF CHEMISTRY

REVIEW

View Article Online
View Journal | View Issue

Check for updates

Cite this: *Nanoscale Adv.*, 2021, **3**, 106

Recent advances in phase change material based nanoplatforms for cancer therapy

Changyu Cao,[a] Nan Yang,[a] Hanming Dai,[a] Han Huang,[a] Xuejiao Song,*[a] Qi Zhang*[c] and Xiaochen Dong *[ab]

Cancer has become a severe threat to human life due to its high mortality and metastatic rate. Effective inhibition and killing of cancer cells using chemotherapeutic drugs have been a promising means in clinical cancer therapy. However, the low selectivity, drug-resistance, uncontrollability and serious side effects of chemotherapy significantly limit its further development. There is an urgent need for new treatment strategies to compensate for deficiencies inherent in chemotherapy alone. A growing body of research shows that combined treatment strategies have the potential to overcome this dilemma by achieving significantly enhanced synergistic effects and reduced side effects. Emerging phase change materials (PCMs) create an ideal nanoplatform for cancer combination therapy due to their universal loading properties, stable and temperature-responsive phase transition capability, and excellent natural biocompatibility/biodegradability. The release of therapeutic agents can be precisely controlled through external, non-intrusive stimuli (such as NIR light and ultrasound), avoiding systemic toxicity associated with conventional chemotherapy. Herein, the construction methods and design principles of PCM-based nanoplatforms serving as strict gatekeeper and smart payload delivery systems are discussed in detail. Moreover, the advantages and disadvantages of these nanoplatforms are provided. A suitable discussion and perspective of the remaining challenges and future opportunities for PCM-based nanoplatforms in cancer treatment are also given in conclusion.

Received 30th July 2020
Accepted 12th November 2020

DOI: 10.1039/d0na00622j

rsc.li/nanoscale-advances

Open Access Article. Published on 13 November 2020. Downloaded on 12/5/2025 12:37:40 AM.
This article is licensed under a Creative Commons Attribution-NonCommercial 3.0 Unported Licence.

1. Introduction

Cancer has caused numerous human deaths, posing a serious threat to human health.[1] Although the efficacy of traditional clinical cancer therapies including surgery, radiotherapy and chemotherapy is rapidly improving, insurmountable limitations cannot be ignored due to complicated mechanisms, diverse tissue structures and easy metastases of malignant tumors. Surgical resection in early-onset solid tumors is effective, but metastatic tumor cells are difficult to remove by this method. Chemotherapy is also a common strategy for clinical cancer treatment. However, commonly used chemotherapeutic drugs would induce damage to normal cells while killing tumor cells, causing serious side effects and resulting in drug resistance in cancer cells. Radiotherapy, using radionuclides or rays (such as X-rays) to irradiate tumors that cause ionizing radiation damage to cancer cells, would cause serious damage to adjacent tissues.[2] Thus, the development of novel cancer treatment methods is particularly urgent.

Various types of novel cancer treatment strategies and methods, such as photothermal therapy (PTT),[3] photodynamic therapy (PDT),[4] chemodynamic therapy (CDT),[5] and sonodynamic therapy (SDT),[6] have been developed to compensate for the lack of traditional therapies. These advanced therapies generally have the characteristics of accurate targeting, remote controllability, high biological safety, low drug-resistance and low trauma. In addition, owing to rapidly developed versatile nanoplatforms, it is possible to integrate different types of payloads within a single system to achieve multi-functionality or multi-mode cancer combination therapies. Compared to that of single-mode treatment, the killing efficiency of cancer cells could be significantly improved, and the severe adverse effects decreased simultaneously. Researchers have dedicated their efforts to finding ideal nanoplatforms which can carry different payloads and preventing them from being pre-released or deactivated during blood circulation. Meanwhile, upon arriving at tumor sites, payloads are expected to be released in a controlled manner under different stimuli, such as light, temperature, pH, or other cancer biomarkers. Hence, nanoplatforms containing the above characteristics may not only combine different functions or therapies within a single system

[a]Key Laboratory of Flexible Electronics (KLOFE), Institute of Advanced Materials (IAM), School of Physical and Mathematical Sciences, Nanjing Tech University (NanjingTech), Nanjing 211800, China. E-mail: iamxcdong@njtech.edu.cn; xjsong@njtech.edu.cn
[b]School of Chemistry and Materials Science, Nanjing University of Information Science and Technology, Nanjing 210044, China
[c]School of Pharmaceutical Sciences, Nanjing Tech University (NanjingTech), Nanjing 211800, China. E-mail: zhangqi@njtech.edu.cn

© 2021 The Author(s). Published by the Royal Society of Chemistry

Open Access Article. Published on 13 November 2020. Downloaded on 12/5/2025 12:37:40 AM.
This article is licensed under a Creative Commons Attribution-NonCommercial 3.0 Unported Licence.

for improved therapeutic effects, but also reduce the off-target toxicity of payloads, thus becoming a research focus.

Phase change materials (PCMs), which have large latent fusion heat and revisable transitions between solid and liquid states, have been widely utilized in thermal energy storage and solar energy applications.[7] More recently, PCMs, particularly those containing natural fatty acids or fatty alcohols, have received considerable interest in acting as thermo-responsive materials for cancer therapy due to their reasonable melting point, low cost, chemical stability, and excellent biocompatibility/biodegradability.[8] Besides, PCMs consisting of eutectic mixtures of fatty acids are increasingly preferred due to their more appropriate and stable melting points (>37 °C) and more satisfactory release rates.[9] Interestingly, emerging therapies, especially PTT, are accompanied by the release of large amounts of heat during the treatment process, with temperatures capable of reaching the phase transition temperature of PCMs. With the introduction of PCMs in emerging therapies accompanied by heat generation, PCMs can not only be utilized as gating materials to prevent pre-release of encapsulated payloads, but also act as stimuli responsive drug carriers for the rapid release of payloads. Xia *et al.* recently reviewed the progress of PCMs in controlled release.[9] Their main focus was on the discussion of PCMs as a temperature-controlled release carrier. We specifically emphasize the design and construction of a PCM-based nanoplatform for combination therapy, including the choice of PCM components, combinations of therapeutic agents and selection of external stimuli. Besides, the problems and deficiencies that may arise from combined nanoplatforms are discussed. In conclusion, the significant progress of PCM-based nanoplatforms in cancer therapy, especially the combination strategies, is summarized (Table 1 and Fig. 1). Meanwhile, insights into the current challenges and further directions in the use of PCMs are provided.

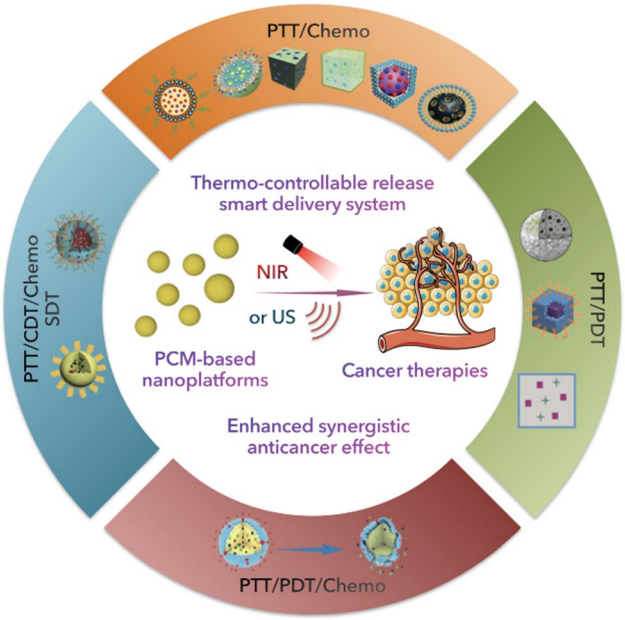

Fig. 1 Schematic diagram of PCM-based nanoplatforms for cancer therapy.

2. PCM-based nanoplatforms for PTT/Chemo combination therapy

Since tumor tissues present poor heat dissipation and tumor cells exhibit low thermal resistance, local hyperthermia has been identified as a potential therapy for the treatment of tumors. In particular, PTT, which can convert light energy to heat to kill cancer cells, has recently attracted extreme attention due to its minimal invasiveness, spatiotemporal control, low drug resistance development, insignificant systemic toxicity and negligible side effects.[10,11] Chemotherapy, as systemic therapy, commonly uses cytotoxic chemotherapeutic drugs to

Table 1 Summary of PCM-based nanoplatforms for cancer combination therapy

Applications	Names	PCM compounds	Therapeutic agent	PATs	Melting points (°C)	Stimulus	Wavelength (nm)	Ref.
PTT/Chemo	DOX/IR780-PCM	Lauric acid/stearic acid	DOX	IR780	39	NIR	808	15
	NPs@BOD/CPT	Lauric acid/stearic acid	CPT-11	lnBOD-Cl	39	NIR	785	16
	Drugs-PCM@AuNCs	1-Tetradecanol	Drugs	AuNCs	38–39	HIFU	—	21
	H_2SeO_3-PCM@AuNCs	Lauric acid	H_2SeO_3	AuNCs	43	NIR	808	22
	AIPH-PCM@AuNCs	Lauric acid	AIPH	AuNCs	44–46	NIR	808	23
	$CaCl_2$-PCM@AuNCs	Lauric acid	$CaCl_2$	AuNCs	43	NIR	808	24
	DOX-PCM@MCN	1-Tetradecanol	DOX	MCN	38–39	NIR	808	35
	DOX-PCM@HMPB	1-Pentadecanol	DOX	HMPB	42	NIR	808	39
	DOX/CPT-PCM@HMPB	1-Tetradecanol	DOX/CPT	HMPB	40–42	NIR	808	42
	DOX/ICG-PCM@SiO_2	Lauric acid/stearic acid	DOX	ICG	39	NIR	808	48
	DOX/PDA-PCM@ZIF8	1-Tetradecanol	DOX	PDA	38–40	NIR	808	58
PTT/PDT	Ce6/NDs–PCM	Lauric acid	Ce6	NDs	46	NIR	670	62
	$sMnO_2$/IR780-PCM	1-Hexadecanol	$sMnO_2$/IR780	IR780	46	NIR	808	63
	ZGC/IR780-PCM	1-Hexadecanol	ZGC/IR780	IR780	45	NIR	808	75
PTT/PDT/Chemo	DPP-BT/DOX-PCM	Lauric acid/stearic acid	DPP-BT/DOX	DPP-BT	39	NIR	730	80
PTT/CDT/Chemo	Fe-GA/Ca_2O-PCM	1-Hexadecanol	Fe-GA/Ca_2O	Fe-GA	46	NIR	808	95
SDT	Fe(VI)/PpIX-PCM@HMON	Lauric acid	Fe(VI)	PpIX	44–46	US	—	104

Open Access Article. Published on 13 November 2020. Downloaded on 12/5/2025 12:37:40 AM.
This article is licensed under a Creative Commons Attribution-NonCommercial 3.0 Unported Licence.

kill tumor cells. Undesirably, normal cells and immune cells are also killed during treatment, causing significant side effects, such as nausea and vomiting to the patient. Worse yet, the generation of drug resistance in cancer cells results in frustration or even failure of chemotherapy treatment. Remarkably, with the introduction of PTT, the thermal effect induced by PTT would disrupt the stability of the cancer cell membrane, increase its permeability, further making cancer cells more vulnerable to chemotherapeutic drugs, achieving enhanced synergistic therapeutic efficacy and reducing the dose of chemotherapeutic drugs accordingly. Hence, the combination of photothermal and chemotherapy exhibits great potential in enhancing anticancer efficacy. Despite the success of combination PTT in alleviating the development of drug-resistance and lowering the dose usage of chemotherapeutic agents, the *in vivo* toxicity of nanoparticles (NPs) formed by self-assembly of photothermal agents (PATs) and chemotherapeutic agents cannot be overlooked due to the lack of effective and stable drug delivery and means of controlled release. Careful design of the delivery system is critical when building a nanoplatform for combination therapy. Generally, an ideal delivery system may have the following features to meet the requirement of clinical applications: (i) simple and versatile construction to load no matter hydrophilic or hydrophobic payloads. (ii) Stable thermal-responsive triggered release within a narrow temperature range (>37 °C). (iii) Strict gating of payloads to ensure no prerelease to avoid off-target toxicity. (iv) Excellent biocompatibility and biodegradability such that it can be degraded and cleared from the body. (v) Low cost, large loading capacity and ease of obtaining and engineering. On this basis, PCMs exhibit great advantages. Chemotherapeutic drugs loaded within PCMs can be well protected from premature release. Besides, PCMs show sensitive responses to temperature variations; therefore, PATs are introduced into PCMs to increase temperature under laser irradiation, finally inducing the release of chemotherapeutic drugs at determined tumor sites.[12–14] In this section, we mainly

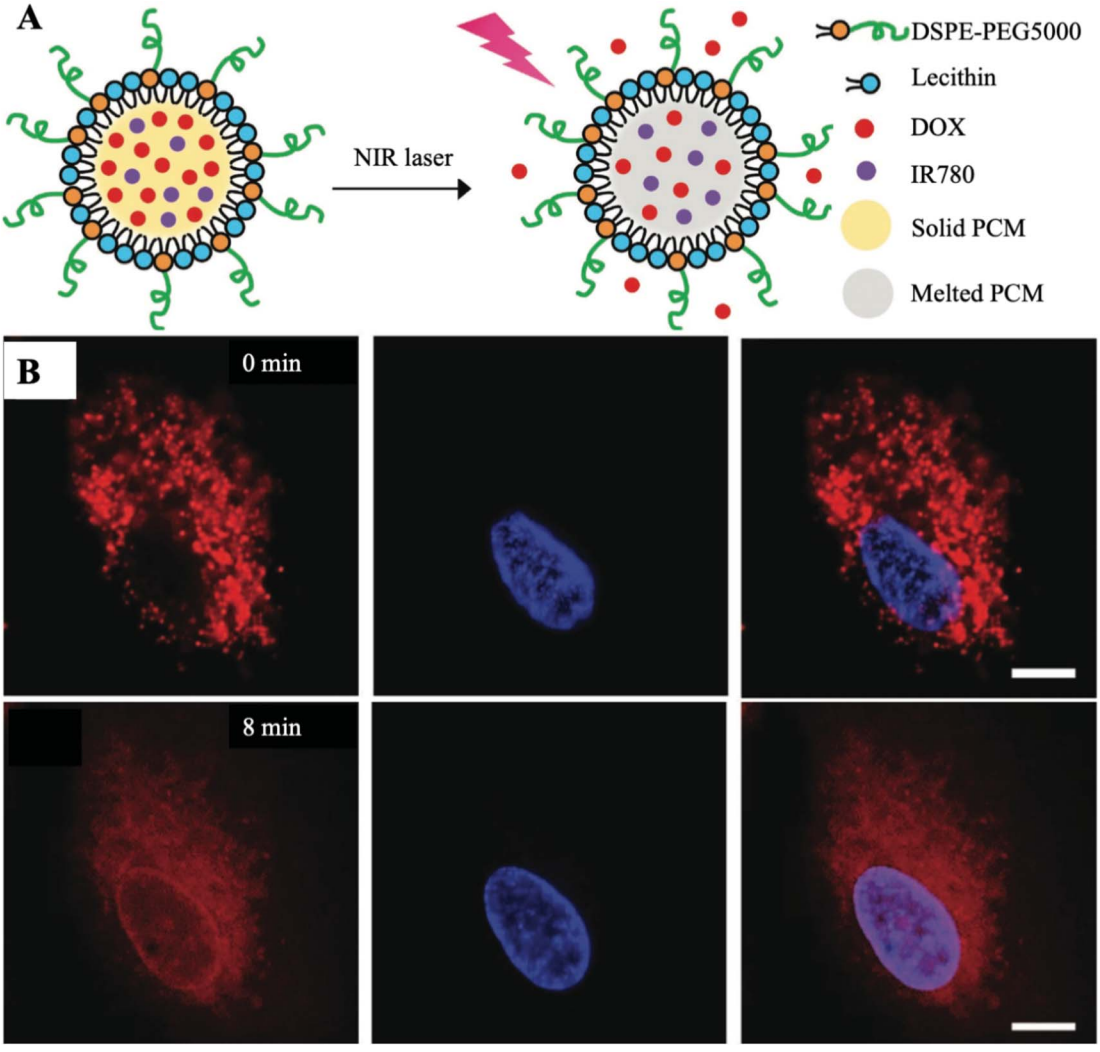

Fig. 2 (A) Schematic description shows the NIR-triggered release of DOX from the melted PCM. (B) Release images of DOX (red) in A549 cells co-incubated with DOX/IR780-PCM NPs under laser irradiation (808 nm, 0.2 W cm^{-2}, 8 min). The nucleus was stained with Hoechst 33342 (blue). Scale bar: 10 μm. Adapted with permission from ref. 15. Copyright 2017 Wiley-VCH.

© 2021 The Author(s). Published by the Royal Society of Chemistry

Open Access Article. Published on 13 November 2020. Downloaded on 12/5/2025 12:37:40 AM. This article is licensed under a Creative Commons Attribution-NonCommercial 3.0 Unported Licence.

summarize a series of PCM-based nanoplatforms for PTT/Chemo combination therapy. The design and construction concepts, core components, advantages and disadvantages of these nanoplatforms are discussed. We also pay particular attention to the cases where PCMs serve as a smart filling system for hollow NPs, mainly including Au nanocages (AuNCs), mesoporous carbon (MCN) NPs, hollow mesoporous Prussian blue (HMPB) NPs, SiO_2 NPs and ZIF-8 NPs, which has been well developed to encapsulate payloads filled with PCMs for thermo-responsive release of anticancer drugs.

2.1 Drug/PAT-PCM nanoplatforms

Xia *et al.* pioneered the loading of the chemotherapeutic drug doxorubicin (DOX) and organic PAT IR780 into a single PCM-based nanoplatform (Fig. 2A).[15] Hydrophilic DOX is clinically administered by injection and is widely used in chemotherapy due to its universal nature in the killing of cancer cells. Unfortunately, the typical clinical dose of DOX would also kill immune cells indiscriminately, resulting in immunosuppression and limited therapeutic efficiency. An emerging PCM has significantly decreased the systemic toxicity of DOX and ensured therapeutic efficacy by perfect protection of the encapsulated drug and strict control of drug release under laser irradiation. In this work, PCMs were prepared from lauric acid and stearic acid (4 : 1, w/w) with a certain melting point at 39 °C. The use of the fatty acid eutectic mixture effectively reduced the crystallinity of the matrix during the coagulation process, which significantly improved the drug loading efficiency compared to that of conventional polymer-based nanocarriers. Additionally, PCMs were modified by anti-solvent precipitation with a mixture of lecithin and 1,2-distearoyl-*sn*-glycero-3-phosphoethanolamine-*N*-[methoxy(poly(ethylene glycol))-5000] (DSPE-PEG) to improve the homogeneity of its dispersion in water as well as its stability, which contributed to the further *in vivo* application of PCMs. Furthermore, amphiphilic PCMs improved the disadvantage of poor solubility of hydrophobic IR780 and enhanced the uptake of IR780 by tumor cells, which in turn enhanced the photothermal effect. The encapsulation of PCMs also prevents premature clearance of IR780 *in vivo*. According to the quantified data on drug release, the amount of released DOX gradually increased with the increasing irradiation time. After co-incubation of DOX/IR780-PCM NPs with cancer model cells (A549 cells) for 3 h, the high fluorescence intensity of DOX was observed, indicating that DOX/IR780-PCM NPs successfully entered the cell under the protection of PCMs and were enriched through the lysosomal pathway. As shown in Fig. 2B, DOX was mainly limited to lysosomes before laser irradiation. And then DOX started moving from the acidic compartment to the cytoplasm upon laser irradiation for 8 min, which further confirmed the successful implementation of the NIR-triggered drug release nanoplatform. These outcomes indicated that NIR laser irradiation could not only trigger the release of DOX by the PCM, but also promote the lysosomal escape of DOX. In addition, this combination therapy can also reduce the dose of DOX in chemotherapy, thereby reducing the toxic effect of DOX on cancer patients. The preparation of the nanoplatform in this work is simple because of the ease of drug loading by the PCM. The rate of release can be controlled using the duration of the laser irradiation and photothermal enhancement of the chemotherapy is finally achieved.

Despite considerable progress made in DOX/IR780-PCM nanoplatforms for reducing the systemic toxicity of anticancer drugs, these NPs encapsulated with PCMs are still unable to achieve effective targeting of tumors. To address this issue, Tian *et al.* reported a specific therapeutic nanoplatform called NPs@BOD/CPT with *in situ* production of H_2S-triggered NIR PATs for on-demand temperature-controlled drug release (Fig. 3A).[16] Since overexpressed H_2S in a tumor microenvironment (TME) has been recognized as a cancer biomarker for a variety of cancers,[17] NPs@BOD/CPT was used to co-encapsulate a reasonably designed boron bipyrrole methylene (InTBOD-Cl) dye (served as H_2S-activated NIR PAT) and clinical anticancer drug camptothecin-11 (CPT-11) with the support of a PCM. Under laser irradiation, InTBOD-Cl showed a minimal photothermal effect without H_2S, and solid NPs@BOD/CPT retained the loaded CPT-11 internally. In contrast, the maximum photothermal performance would be achieved in the presence of H_2S. The local temperature increasing above the melting point (39 °C) caused the transient release of captured drug CPT-11, finally achieving effective treatment of cancer. As shown in Fig. 3B, under laser irradiation, in the presence of H_2S, the temperature increased by about 18 °C, demonstrating that H_2S can effectively convert InTBOD-Cl to high-performance PAT InTBOD-SH. Encouraged by the high photothermal performance of NPs@BOD/CPT, the effect of NPs@BOD/CPT on the release of CPT-11 under the control of H_2S and laser irradiation was subsequently estimated (Fig. 3C). Long-term laser irradiation will increase the release of CPT-11 in the presence of H_2S. However, in the absence of H_2S, quite a few drugs were identified to be released from NPs@BOD/CPT with laser irradiation, indicating that NPs@BOD/CPT nanoplatforms without H_2S activation exhibited less photothermal properties and could not cause the melting of PCMs, reflecting the excellent on demand thermal ability of this platform in targeting tumors. According to *in vivo* cancer treatment after *in situ* injection (Fig. 3D), since a PAT was not present in NPs@CPT, there was no apparent inhibition of the tumor in the NPs@CPT and laser irradiation group, showing that the loaded drug was effectively retained within the solid matrix. The tumors of mice in the NPs@BOD/CPT treatment group were completely suppressed after laser irradiation and did not recur, indicating powerful application potential of NIR laser control combination therapy for specific activation of NPs@BOD/CPT. In fact, the targeting of tumors was attributed to the dual activation of H_2S and photothermolysis. By using H_2S overexpression in the TME to distinguish normal cells, the weak photothermal PAT InTBOD-Cl in the tumor cells was converted to higher NIR absorption PAT InTBOD-SH, and when under laser irradiation, the heat absorbed in the normal cells was not sufficient to reach the melting point of the PCM, which ultimately resulted in the release of chemotherapeutic drugs mostly in tumor cells. Under PCM encapsulation, inactivated NPs@BOD/CPT would not release CPT-11 to cause damage to normal cells. More

Open Access Article. Published on 13 November 2020. Downloaded on 12/5/2025 12:37:40 AM.
This article is licensed under a Creative Commons Attribution-NonCommercial 3.0 Unported Licence.

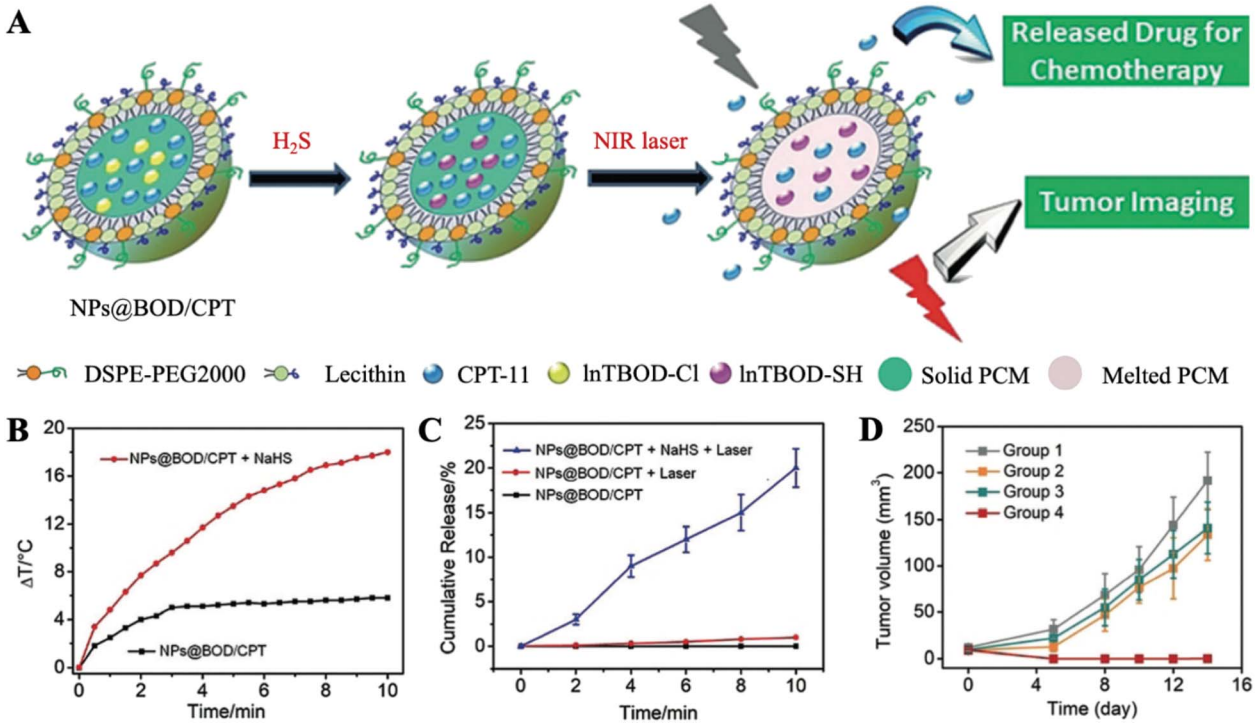

Fig. 3 (A) Schematic diagram of H_2S targeting NPs@BOD/CPT for cancer on-demand light-controlled drug release. (B) Temperature rise curves of NPs@BOD/CPT in the absence and presence of NaHS. (C) Cumulative CPT-11 release curves of NPs@BOD/CPT (785 nm, 5.12 W cm^{-2}) after different treatments. (D) Tumor growth curves of HCT116 tumor-bearing mice in different treatment groups. Adapted with permission from ref. 16. Copyright 2019 Wiley-VCH.

importantly, PCMs solved the clinical problem of reduced antitumor activity after CPT-11 was made into a water-soluble sodium salt while improving the uptake of cancer cells. The advantage of this platform is that it does not introduce other functional components, and only changes the conditions for the PAT to achieve photothermal triggering in tumors. This inspires researchers to design and synthesize PATs with a TME-specific response to the first activation.

2.2 Drug-PCM@AuNC nanoplatforms

Hollow nanostructures of precious metals, such as gold nanocages (AuNCs), show robust absorption capacities at 700–900 nm and are often used as promising PATs.[18–20] Compared to organic PATs, AuNCs do not undergo photoquenching and can stably convert light into heat to achieve satisfactory photothermal effects. In addition, AuNCs have a stable structure and strong loading capacity. Therefore, AuNCs have inherent advantages for constructing PCM-based nanoplatforms. Moreover, since the preparation of AuNCs is often coated with a hydrophilic polymer, such as polyvinylpyrrolidone (PVP), it is only generally suitable for hydrophilic drugs. An amphipathic PCM loaded with anticancer drugs packed into the hollow interior of AuNCs successfully addresses the issue for packaging both hydrophilic and hydrophobic drugs.

On this basis, as shown in Fig. 4A, Xia *et al.* offered a facile and versatile strategy, and they creatively used PCMs for packaging various types of therapeutic agents, such as anticancer drug DOX, H_2SeO_3, AIPH and Ca^{2+}. After being mixed well, the PCM and payloads were then packed in the interior of AuNCs.[21–24] It is known that the choice of therapeutic agents has shifted from initial anti-cancer drugs to new therapeutic agents with lower drug-resistance generation, demonstrating broad application prospects. For Drug-PCM@AuNCs, in this work, they selected 1-tetradecanol for making a PCM with melting points at about 38–39 °C. The TEM images showed a noteworthy change in the contrast to those of the AuNCs co-loaded with the Drug-PCM (Fig. 4B and C). As shown in Fig. 4D, the amount of drugs released at room temperature or 37 °C was very limited, which could be attributed to the capture effect of the solid-state PCM. In contrast, when the temperature reached 40 °C, approximately 28% of the packaged drugs were released from AuNCs. As the most important function of PCMs, these experimental results showed that the PCM-based releaser can be easily and stably prepared in AuNCs. All in all, they combined the unique capabilities of AuNCs and PCMs to provide a temperature-regulated drug release smart nanoplatform. Followed by this work, they moreover packed selenite into the AuNC cavity with PCMs. During the process of cell endocytosis, AuNCs can act as carriers and then be employed as PATs to melt lauric acid under NIR laser irradiation, triggering the rapid release of selenite for eventual photothermal-enhanced chemotherapy for cancer cells. Based on the universality of the drug released by this nanoplatform, they also mixed the initiator with the PCM and packed it into the cavity of the AuNCs. Under the NIR laser irradiation, due to the

© 2021 The Author(s). Published by the Royal Society of Chemistry

Open Access Article. Published on 13 November 2020. Downloaded on 12/5/2025 12:37:40 AM.
This article is licensed under a Creative Commons Attribution-NonCommercial 3.0 Unported Licence.

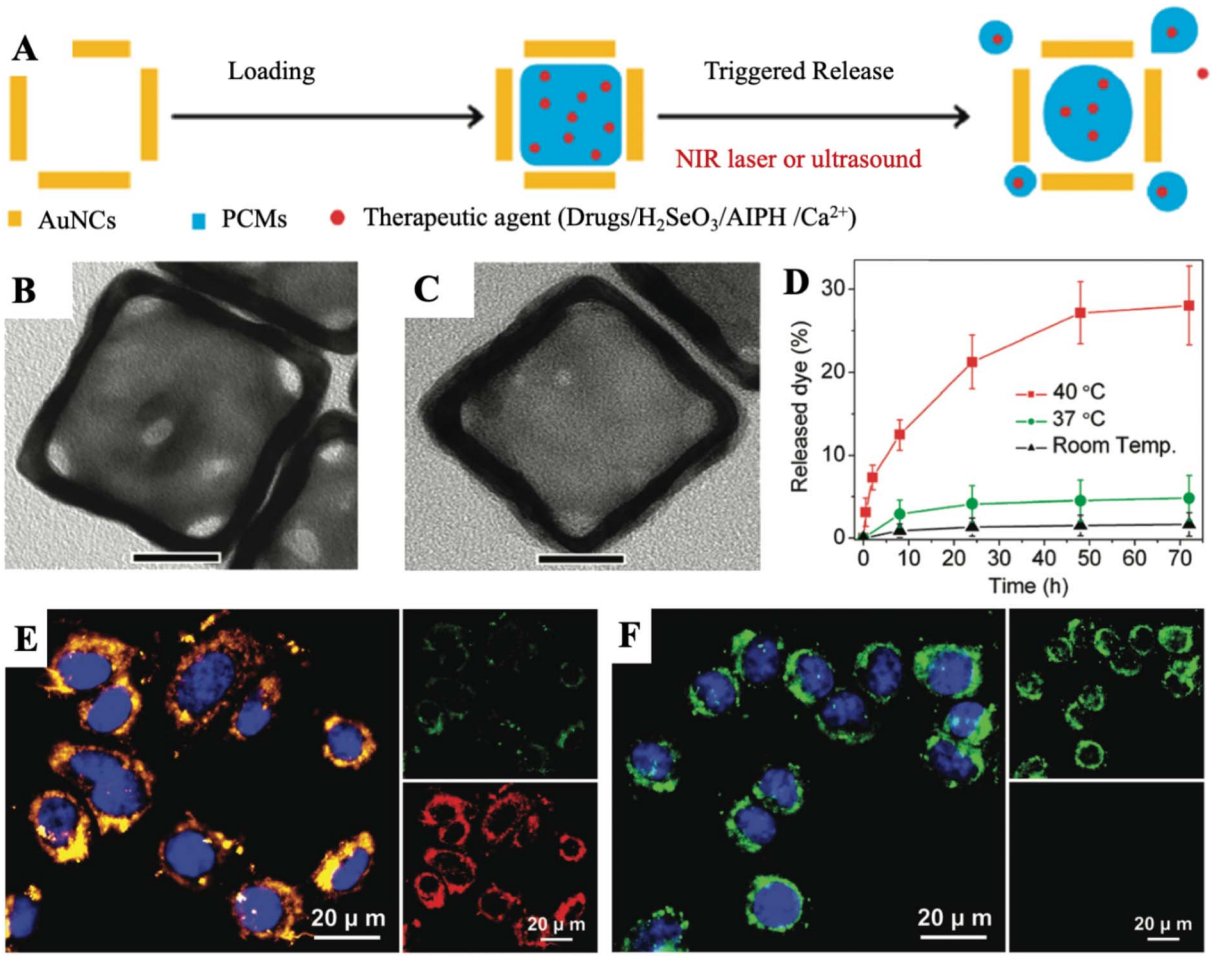

Fig. 4 (A) Schematic diagram of the internal loading and triggered release of therapeutic agents encapsulated with PCMs in AuNCs. The therapeutic agents can be anticancer drugs, H_2SeO_3, AIPH and Ca^{2+}. (B and C) Typical TEM images of AuNCs before and after encapsulating the PCM and payloads. Scale bar: 20 nm. (D) The release curve of dye when heated to different temperatures. Adapted with permission from ref. 21. Copyright 2011 American Chemical Society. (E and F) Fluorescence images of the JC-1 stained A549 cells in the presence or absence of the laser irradiation after being incubated with $CaCl_2$-PCM@AuNCs for 6 h (808 nm, 0.8 W cm^{-2}, 10 min). JC-1 would emit red fluorescence when forming the J-aggregated state and emit green fluorescence when in monomeric form. The nuclei were stained with DAPI in blue. Adapted with permission from ref. 24. Copyright 2019 Wiley-VCH.

photothermal effect of the AuNCs, the PCM melted, causing the loaded initiator to be released and decomposed to generate free radicals. Free radicals generated in this way were very effective in inducing cell apoptosis in hypoxic cancer cells. These therapeutic agents are mainly proposed to solve the problem of TME hypoxia, which limits the efficacy of chemotherapy. Many oxygen-independent therapeutic agents are easily inactivated under complicated physiological conditions. Therapeutic agents directly loaded in AuNCs often prerelease and are eliminated before being enriched at the tumor site. The emergence of PCMs allows these powerful therapeutic agents to maintain excellent therapeutic activity before reaching the lesion. Upon laser irradiation, therapeutic agents will be released to a large extent in a hypoxic environment to achieve enhanced efficacy of chemotherapy.

Different from the exogenous therapeutic agents mentioned above, endogenous Ca^{2+}, as an important component of bone and other tissues, has been seen as an ideal promising drug candidate for future therapeutic applications due to its antitumor effect.[25,26] A significant increase in the intracellular Ca^{2+} concentration will cause cell death by abolishing nucleic acids and intracellular proteins.[27] However, it is difficult to transfer highly charged Ca^{2+} into living cells and increase its intracellular concentration to lethal levels because cells can precisely adjust the concentration of Ca^{2+} in living cells to maintain balance.[28–30] Therefore, a suitable Ca^{2+} nanocarrier is needed to be designed. Xia *et al.* combined AuNCs with a PCM based their previous research, developing a suitable nanoplatform for delivery and controlled release of intracellular Ca^{2+} under NIR irradiation. $CaCl_2$ (as the source of Ca^{2+}) was co-dissolved with a PCM and then loaded into the cavity of AuNCs to prepare $CaCl_2$-PCM@AuNC NPs. The PCM existed in a solid state without NIR irradiation, and $CaCl_2$ could be completely encapsulated in the PCM without leakage in advance. After cell internalization, $CaCl_2$-PCM@AuNC NPs did not show adverse effects because the small increase in intracellular Ca^{2+}

© 2021 The Author(s). Published by the Royal Society of Chemistry

Open Access Article. Published on 13 November 2020. Downloaded on 12/5/2025 12:37:40 AM.
This article is licensed under a Creative Commons Attribution-NonCommercial 3.0 Unported Licence.

concentration caused by the slow biodegradation of the PCM was insufficient to induce cytotoxicity without NIR irradiation. However, due to the temperature rise caused by the photothermal effect of AuNCs under laser irradiation, the PCM rapidly melted, resulting in the quick release of Ca^{2+}. The rapid generation of intracellular Ca^{2+} can trigger cytotoxicity and eventually cause cell apoptosis (Fig. 4E and F). With its good biocompatibility and controllable release, the $CaCl_2$-PCM@AuNC nanoplatform is expected to have potential application in combined cancer treatment with reduced side effects. This work provides a new perspective for the realization of chemotherapy by changing the concentration of endogenous Ca^{2+}, making the originally non-toxic Ca^{2+} produce strong cytotoxicity to cancer cells.

2.3 Drug-PCM@MCN nanoplatforms

Although AuNCs have been successfully applied to PCM-based nanomedicine loads, the long term toxicity of gold cannot be ignored.[31,32] Similar to AuNCs, mesoporous carbon (MCN) NPs possess good drug loading capability, large surface area and adjustable drug release properties. In addition, MCN NPs demonstrate good dispersibility in aqueous media after carboxylation and have a satisfactory photothermal effect.[33,34] Guo *et al.* recently prepared a novel type of nanocarrier composed of MCN NPs, in which DOX was supported in the unique mesoporous structures of MCN (Fig. 5A).[35] Under NIR laser irradiation, the maximum amount of DOX can be observed in the nucleus, thereby producing a sufficient cytotoxic effect to significantly kill tumor cells. The increase in purple fluorescence indicated that the photothermal effect further induced an increased release of the DOX. In addition, this also confirmed the successful NIR-triggered release of DOX from the holes of the MCN NPs with the support of the PCM. Compared to AuNCs, MCN NPs exhibit lower toxicity, similar loading capacity and better water solubility. But their stability is slightly worse. On the other hand, the PCM remains as a temperature-controlled release material for filling MCN apertures, allowing MCN carriers to overcome premature leakage. And the MCN NPs have an ordered mesoporous pore structure with precisely tunable pore sizes in the range of 3–10 nm, allowing the NIR-triggered release rate to be precisely tuned.

2.4 Drug-PCM@HMPB nanoplatforms

Prussian blue (PB)-based NPs are also promising candidates for PATs due to their great biological safety, good photostability, strong NIR region absorption and high photothermal

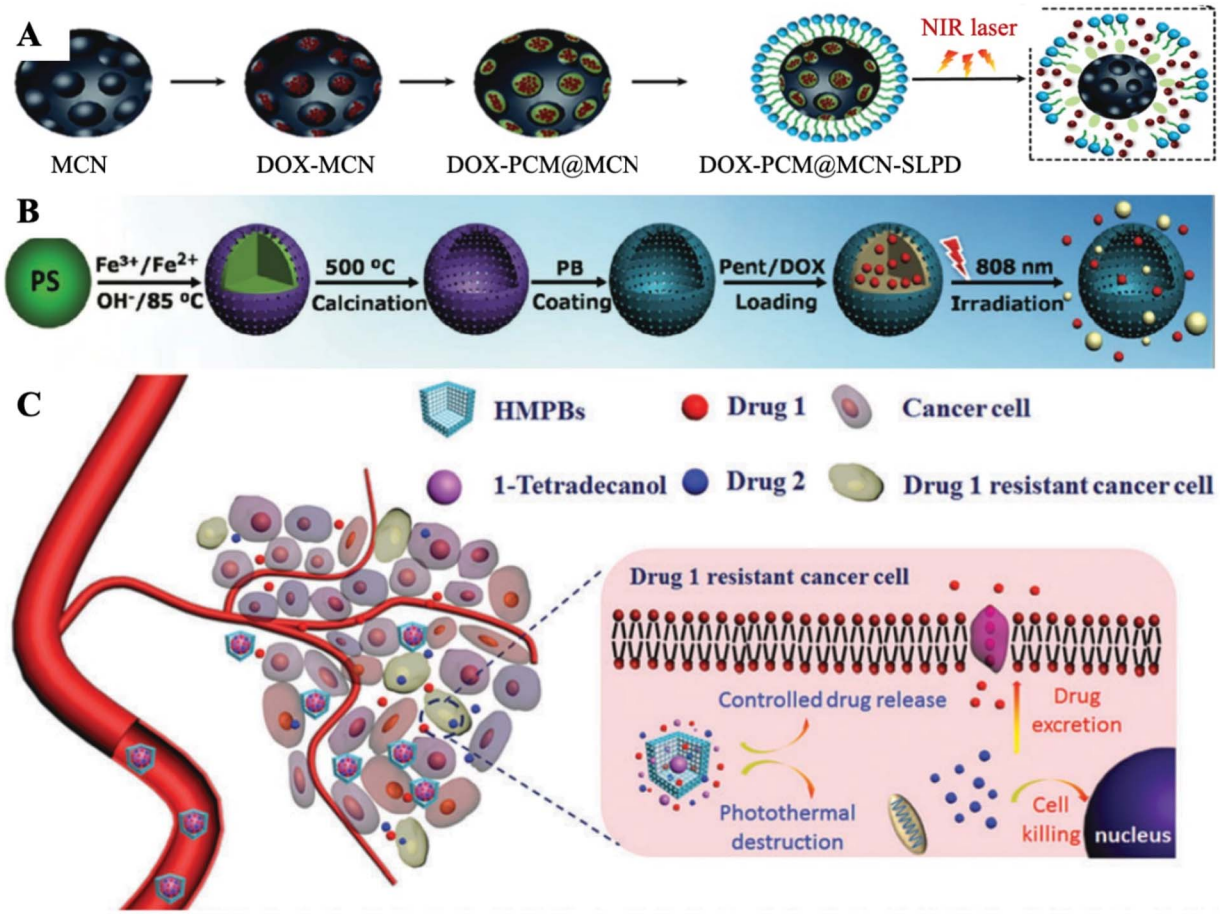

Fig. 5 (A–C) Schematic diagram of the design of DOX-PCM@MCN, DOX-PCM@HMPB and DOX/CPT-PCM@HMPB nanoplatforms for PTT/Chemo combination therapy. Adapted with permission from ref. 35. Copyright 2019 The Royal Society of Chemistry, ref. 39. Copyright 2017 Wiley-VCH, and ref. 42. Copyright 2017 The Royal Society of Chemistry, respectively.

© 2021 The Author(s). Published by the Royal Society of Chemistry

Open Access Article. Published on 13 November 2020. Downloaded on 12/5/2025 12:37:40 AM.
This article is licensed under a Creative Commons Attribution-NonCommercial 3.0 Unported Licence.

conversion efficiency.[36] Meanwhile, chemotherapy based on anticancer drugs is used in combination to obtain better therapeutic effects for PB-based PTT.[37] To reduce the risk of leakage of antitumor drugs in advance, lengthening the circulation time of drugs in blood is a practical strategy.[38] Cai *et al.* manufactured PCM protected hollow PB NPs (HMPB) to load with drugs for PTT/Chemo combination therapy (Fig. 5B).[39] 1-Pentadecanol (Pent) was used to make the PCM for loading/locking anticancer drug DOX, realizing nearly "zero release", which greatly reduced the toxic and severe side effects of DOX before reaching tumor lesions. The DOX-PCM@HMPB nanoplatform showed a heat-dependent drug release profile. The amount of released DOX at 20 and 37 °C is hardly negligible (<5%), while the amount of DOX released at 45 °C is over 80%. As a result, they finally achieved a true "on–off" pulsatile drug release manner by turning the applied NIR laser on or off. More importantly, by simultaneously directing different signalling pathways to prevent oncogene mutations and reduce acquired drug-resistance, the combination of two or more anticancer drugs in a single system has been a method of combating drug-resistance clinically.[40,41] To date, although great developments have been made to investigate different nanoplatforms for co-delivering different anticancer drugs together to tumor lesions, there is still an urgent need to design a novel drug delivery nanoplatform with controlled drug release properties. Zha *et al.* introduced a PCM into HMPB to co-deliver and control the release of two different anticancer drugs under NIR laser irradiation to overcome drug resistance and prevent the release of drugs into healthy tissues to avoid unnecessary cytotoxicity (Fig. 5C).[42] Herein, they used DOX and CPT as two model anticancer drugs. A Drugs-PCM@HMPB nanoplatform was built by embedding DOX and CPT together inside the PCM, and then loading the PCM into the hollow interior of HMPB. Owing to the protection of the solid state of 1-tetradecanol under physiological conditions without NIR laser irradiation, the Drugs-PCM@HMPB nanoplatform can achieve "zero release" of the drugs. In addition, the timing of laser irradiation can be selected according to the drug release curve of the Drugs-PCM@HMPB nanoplatform to release anticancer drugs to overcome drug-resistance. More importantly, owing to the generation of heat, the uptake of drugs by cells can be greatly improved through increasing membrane fluidity and cell metabolism, and the prepared Drugs-PCM@HMPB nanoplatform demonstrated a significant synergistic cancer killing effect. This work proposes a strategy to combat drug resistance by using dual anti-cancer drugs in a single PCM-based nanoplatform due to the amphiphilic nature of the PCM. The combination drug delivery strategy takes advantage of the fact that cancer cells have different sensitivities to drugs to reduce drug-resistance generation and increase the efficacy of treatment. However, this work overlooks the huge risks associated with the centralized delivery of multiple anticancer drugs,

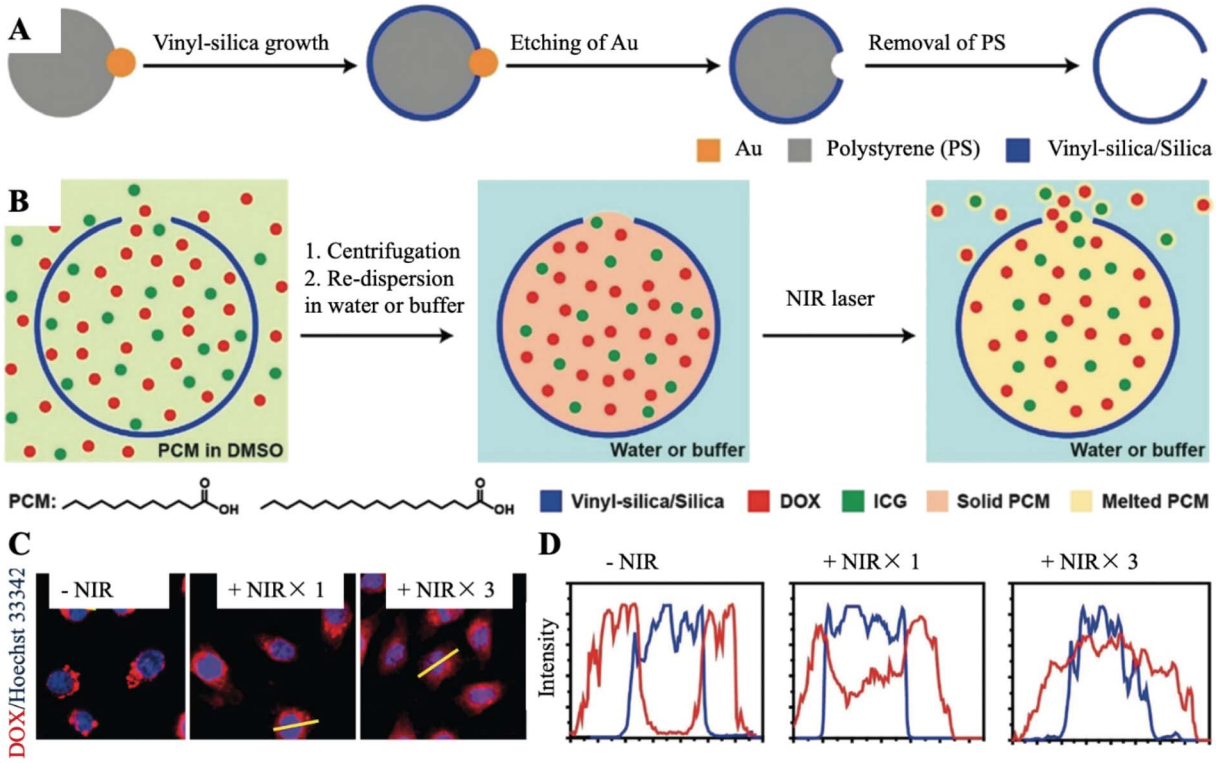

Fig. 6 (A) The synthesis process of SiO_2 nanocapsules with a well-defined hole. (B) Schematic diagram of the encapsulation of a PCM in SiO_2-loaded nanocapsules for temperature-regulated drug release. (C) Fluorescence images of HeLa cells incubated with DOX/ICG-PCM@SiO_2 with and without laser irradiation. The nuclei were stained with Hoechst 33342 in blue and DOX emitted red fluorescence. (D) The corresponding fluorescence intensities of Hoechst 33342 (blue line) and DOX (red line) in HeLa cells. Adapted with permission from ref. 48. Copyright 2019 Wiley-VCH.

© 2021 The Author(s). Published by the Royal Society of Chemistry

Open Access Article. Published on 13 November 2020. Downloaded on 12/5/2025 12:37:40 AM.
This article is licensed under a Creative Commons Attribution-NonCommercial 3.0 Unported Licence.

which may lead to toxic side effects and drug–drug interactions. We envision a future reorientation of this strategy towards the development of PCMs with multiple phase change temperatures. Since a PCM is a mixture of components with different phase change temperatures, the release of different drugs can be achieved by adjusting the intensity of NIR irradiation at different stages of treatment and significantly reducing the risk and burden on the patient.

2.5 Drug/PAT-PCM@SiO_2(ZIF8) nanoplatforms

SiO_2 NPs can be easily modified with other functional groups such as targeting moieties due to their unique structure.[43,44] Importantly, SiO_2 is commonly considered a biocompatible material that will be self-removed from the human body after treatment, making it appealing for future clinical transformation.[45–47] Unfortunately, SiO_2 NPs themselves do not have a photothermal effect, and the introduction of PATs is necessary. Xia *et al.* recently reported a new method for temperature-controlled drug release by utilizing SiO_2 NPs with well-defined pores (Fig. 6A and B).[48] A fatty acid made PCM, anticancer drug DOX and PAT indocyanine green (ICG) were easily loaded into internal SiO_2 NPs through the surface pores. DOX would release from the pores in an artificially controlled manner when activated by the photothermal effect supported by the ICG. The amount of released payloads was positively related to the scope of the holes or the period of laser exposure (Fig. 6C and D). A PCM packaged in SiO_2 NPs has many benefits, including easy modification, enhanced stability, artificially controlled release and the capability to load other multi-functional components.

In recent years, biodegradable nano-metal organic framework materials (NMOFs) have been widely used as new smart drug delivery carriers,[49,50] because the metal ions and the coordinate organic linking group can be adjusted to obtain the

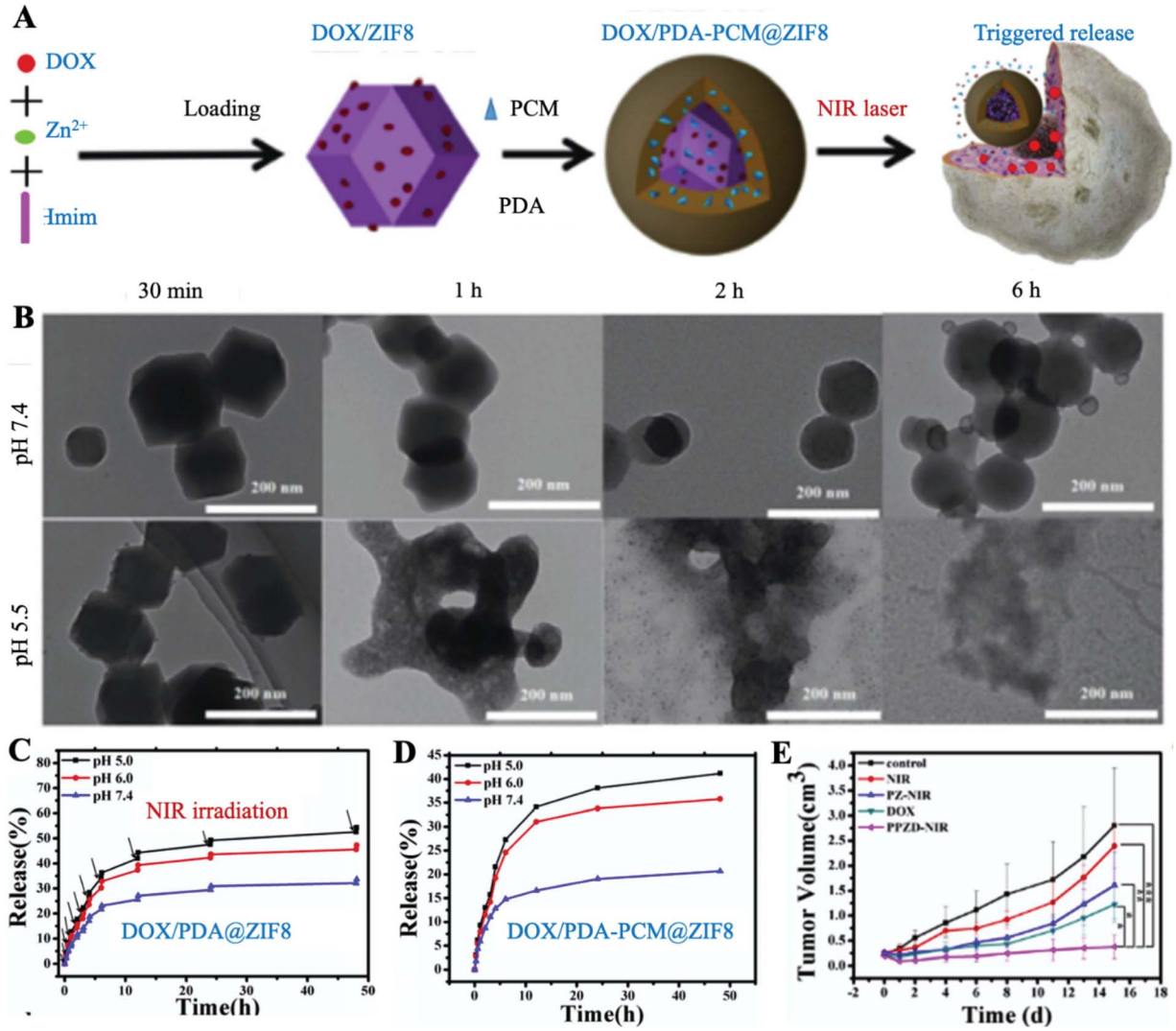

Fig. 7 (A) Schematic shows the synthesis of DOX/PDA-PCM@ZIF-8 and NIR-triggered release of DOX. (B) Degradation of DOX/PDA-PCM@ZIF-8 at different time points under different pH conditions. (C) Controlled release of DOX in DOX/PDA@ZIF8 at different pH upon laser irradiation. (D) pH-sensitive release performance of DOX/PDA-PCM@ZIF8. (E) Tumor growth in different treatment groups. PZ, and DOX/PDA@ZIF8; PPZD, and DOX/PDA-PCM@ZIF8. Adapted with permission from ref. 58. Copyright 2018 Elsevier Ltd.

© 2021 The Author(s). Published by the Royal Society of Chemistry

Open Access Article. Published on 13 November 2020. Downloaded on 12/5/2025 12:37:40 AM.
This article is licensed under a Creative Commons Attribution-NonCommercial 3.0 Unported Licence.

desired characteristics.[51–54] Zeolitic imidazolate frameworks (ZIFs) as a subclass have been a potential pH-sensitive nanocarrier for anticancer drugs.[55] They can exist stably in a complex physiological environment and happen to be degraded until transported to TME acidic conditions.[56] However, an unmodified ZIF is highly toxic and cannot distinguish normal cells from tumor cells.[57] Zhong *et al.* designed a PCM-based nanoplatform named DOX/PDA-PCM@ZIF8 for PTT/Chemo combination therapy, which successfully controlled its degradation and reduced its toxicity, making it useful for drug carriers (Fig. 7A).[58] Under NIR laser irradiation, the drug carrier ZIF-8 rapidly degraded specifically under acidic conditions at the tumor site and released DOX in large quantities (Fig. 7B–D). Only under the dual activation of NIR and pH, the release of DOX was then maximized. The acid degradation of ZIF-8 and the thermal fusion of the PCM enable this platform to exhibit excellent tumor-specific therapeutic capabilities. As expected, the DOX/PDA-PCM@ZIF8 + NIR group achieved the best therapeutic efficacy (Fig. 7E). Besides, benefiting from the effective protection of the PCM, the toxicity of ZIF-8 could be decreased to the least, which greatly improved the biosafety of ZIF-based nanocarriers. It is based on this protective property of PCMs that the modified nanocarriers are transformed from toxic to nearly non-toxic, which makes it possible to use carriers for cancer therapy that were previously excellent drug carriers but toxic.

The above-constructed PCM-based nanoplatforms successfully resolved the two specific problems of chemotherapy including high systemic toxicity and low tumor targeting. The components in the PCM-based nanoplatforms show excellent biodegradability, which makes them easy to degrade and clear. However, unnecessary release cannot be avoided during the treatment process. In addition, PCMs with high fatty acids or fatty alcohols are directly exposed to blood, which may cause thrombosis and atherosclerosis after long-term use. Hence, different strategies should be developed to solve these problems: (i) further improvement of the loading capacity of drugs in PCM-based nanoplatforms; (ii) avoidance of direct *in vivo* exposure of PCMs; (iii) alternatives of stable organic PATs to avoid photo quenching; (iv) co-loading multiple anti-cancer drugs, combining other therapies or enhancing photothermal performance to significantly achieve a synergistic effect; (v) introduction of imaging technologies for monitoring, guidance and evaluation of treatment; (vi) joining of endogenous and exogenous stimuli to achieve accurate targeted therapy.

3. PCM-based nanoplatforms for PTT/PDT combination therapy

PDT is a non-invasive cancer treatment, and absorbs light energy to activate photosensitizers (PSs) to generate cytotoxic reactive oxygen species (ROS). Commonly used PSs are organic small molecules, such as Food and Drug Administration (FDA) approved ICG. Although organic PSs exhibit good biocompatibility, the aggregation-caused quenching (ACQ) of most organic PSs under aqueous conditions, poor stability, severe photodegradation and low accumulation at tumor sites would reduce the therapeutic efficiency of PDT.[59] On the other hand, the amount of oxygen at tumor sites is a key factor affecting the generation of ROS.[60] Unfortunately, due to the infinite proliferation of cancer cells and the abnormal growth of blood vessels, most tumors tend to form local hypoxic regions,[61] resulting in the resistance of cancer cells to PDT.

To maintain the stability of PSs during blood circulation and achieve responsive release when they reach the tumor site, Choi *et al.* successfully designed a PCM-based nanoplatform to load nanodiamonds (NDs, PATs) and chlorin e6 (Ce6) (Ce6/NDs-PCM NPs).[62] Ce6/NDs-PCM NPs exhibited a temperature-sensitive "switch", allowing the artificially precise and the controllable release of Ce6. The melting point of the synthesized PCM was 43.8 °C. When the temperature was lower than the melting point, the Ce6/NDs-PCM NPs were solid state, which effectively prevents the premature release of Ce6. Interestingly, the temperature of Ce6/NDs-PCM NPs could rapidly rise to 45.0 °C with laser irradiation, resulting in the phase change of the PCM and controlled release of Ce6. Taking advantage of the protection of the PCM, the stability of Ce6 and the $^1O_2$ production capacity could be effectively improved.

To further apply the wax-seal effect of the PCM, our group manufactured a PCM-based nanoplatform by using an oleic acid (OA) and 1-hexadecanol (Hex) mixture for afterglow imaging-guided controllable PTT/PDT combination therapy.[63] Introducing optical imaging during PDT can not only improve the therapeutic effect but also monitor the effectiveness of the treatment in real-time. Among the developed optical imaging methods, afterglow imaging has received widespread attention as a new technique for autofluorescence-free bioimaging. Commonly used persistent luminescence (PersL) materials for afterglow imaging, such as nano-zinc gallogermanates are still suffering some limitations including poor tumor targeting and severe quenching of PersL in aqueous environments by water or oxygen.[64–68] The emergence of PCMs provides an ideal approach for solving the above difficulties. In short, through capturing $ZnGa_{1.996}O_4$:$Cr_{0.004}$ (ZGC, PersL agents) NPs and IR780 together into a PCM, a multi-functional therapeutic nanoplatform (ZGC/IR780-PCM, Fig. 8A) was then synthesized. Due to the carefully wax-seal of the intact PCM, this nanoplatform effectively prevented quenching of the ZGC NPs and avoided the premature initiation of PDT. SEM images showed that the formation of the ZGC/IR780-PCM was decomposed into formless fragments under NIR laser irradiation, which confirmed that PCMs were previously controlled to melt and decompose caused by a laser exposed to IR780. Notably, the photobleaching effect of IR780 could be effectively reduced owing to the strict protection of the PCM coating. The temperature of the ZGC/IR780-PCM dispersion solution increased by about 15 °C, while free IR780 showed almost no temperature rise (<3 °C). Under NIR laser irradiation, the ZGC/IR780-PCM group achieved the best PersL performance compared with others in water. The PersL intensity of ZGC-PCM NPs increased almost 2.2-fold compared with that of free ZGC NPs owing to the excellent protection of the PCM.[69] More importantly, the PCM truly served as an on–off switch for controlled PDT by preventing interaction between the internal IR780 and the complex external physiological environment. Therefore, NIR and

Open Access Article. Published on 13 November 2020. Downloaded on 12/5/2025 12:37:40 AM.
This article is licensed under a Creative Commons Attribution-NonCommercial 3.0 Unported Licence.

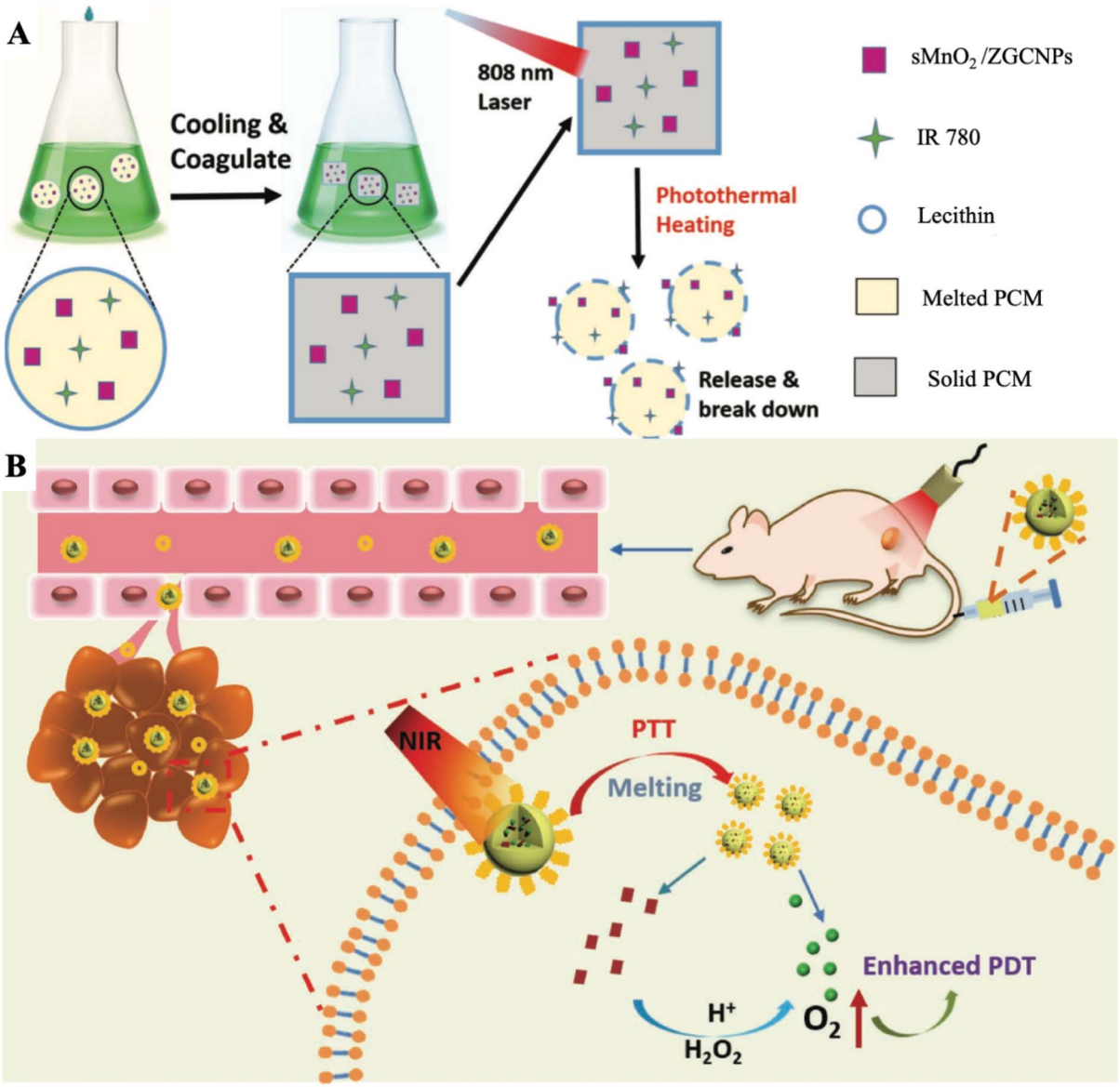

Fig. 8 (A) Schematic diagram of the ZGC/IR780-PCM nanoplatform used to enhance afterglow imaging and photothermally triggered persistent PDT. Adapted with the permission of ref. 63. Copyright 2018 Wiley-VCH. (B) Schematic representation of the formation of the $sMnO_2$/IR780-PCM nanoplatform and the process of responsive tumor hypoxia regulation for enhanced PDT. Adapted with permission from ref. 75. Copyright 2019 Wiley-VCH.

PersL could continuously stimulate the generation of ROS, providing persistent therapeutic effects.[70] These diagnosis-integrated cancer treatment platforms enable monitoring and guidance of the cancer treatment process due to the wax-seal of PCMs, which avoids quenching due to the physiological environment.

Previous studies have shown that tumor hypoxia could be relieved by the use of an appropriate catalyst to decompose the overexpressed endogenous hydrogen peroxide (H_2O_2) to generate oxygen. Most catalysts used to improve tumor oxygenation are not always hermetically sealed, leading to continuous H_2O_2 consumption and oxygen generation before laser irradiation. Pre-generated oxygen is almost consumed by cell activity and spread outside the TME, which significantly reduces the utilization rate of oxygen.[71–74] Hence, our group prepared $sMnO_2$/IR780-PCM NPs by loading IR780 and ultra-small MnO_2 NPs into a PCM with a melting point of 46 °C (Fig. 8A and B).[75] Similar to the previous mechanism, IR780 was packaged inside the PCM to ensure isolation from external water and oxygen, thereby effectively reducing photooxidative bleaching and improving the optical stability of IR780. Meanwhile, the temperature controlled phase transition of $sMnO_2$ based on PCMs can realize light control of oxygen generation, which made the designed nanoplatform no longer limited to the hypoxic conditions of the tumor site and easily achieved high ROS generation efficiency. The photothermal effect caused by IR780 induced the melting of the PCM, thereby exposing $sMnO_2$ to H_2O_2 for increasing the oxygen concentration. In contrast, the oxygen concentration tended to remain stagnant without laser irradiation. Furthermore, the expression intensity of HIF-1α at tumor sites treated with the

© 2021 The Author(s). Published by the Royal Society of Chemistry

Open Access Article. Published on 13 November 2020. Downloaded on 12/5/2025 12:37:40 AM.
This article is licensed under a Creative Commons Attribution-NonCommercial 3.0 Unported Licence.

$sMnO_2$/IR780-PCM NP and laser irradiation group was greatly decreased, showing that $sMnO_2$/IR780-PCM NPs have an effective thermal-responsive tumor hypoxic remission ability. The treatment results of tumor-bearing mice showed that the surface temperature of the tumor can rise to about 49 °C. Such a high temperature is enough to trigger the melting of the PCM, thus releasing $sMnO_2$ and further improving the tumor oxygenation. The resected tumor images further verified that the $sMnO_2$/IR780-PCM NP and laser irradiation treatment group obtained the best treatment effect. In general, the stable strict protection for PSs and thermal-sensitive controlled release properties of PCMs greatly enhance the photostability of PSs and reduce photodegradation, further expanding the use of hydrophobic PSs and increasing the amount of *in situ* oxygen production. Suitable nanoplatforms could greatly broaden the application range of enhanced photodynamic combined photothermal therapy. Notably, due to the limitation of the penetration depth in the NIR-I biowindow, the efficacy of PDT for deeper tumors is still limited. The development of both non-oxygen-dependent and strong NIR-II absorption PSs is a future direction.

4. PCM-based nanoplatforms for PTT/PDT/Chemo combination therapy

The combination of PTT, PDT, and chemotherapy based on PCM-based nanoplatforms has recently attracted considerable attention. The multi-mode diagnosis and treatment platform has become a trend in the field of cancer treatment for the future. The overwhelming advantage of this type of nanoplatform is that it can easily achieve significant combined antitumor efficacy triggered by single NIR laser irradiation. Overall, PCM-based PTT/PDT/Chemo combination therapy delivers a pioneering strategy to design and build all-in-one nanoplatforms for clinical treatment.[76–79] Fan *et al.* designed and prepared a novel type of small molecule dye based on diketopyrrolopyrrole (DPP) named DPP-BT, which showed excellent multifunctional properties.[80] The DPP-BT molecule can not only serve as an agent for NIR-II fluorescence and a photoacoustic imaging (PAI) agent, but also as a PTT/PDT combined therapeutic agent. By co-encapsulating hydrophobic DPP-BT and DOX with a biocompatible PCM, the NPs named P(DPP-BT/DOX) were finally synthesized (Fig. 9A). Under NIR laser irradiation, P(DPP-BT/DOX) NPs can simultaneously generate high PA and NIR-II fluorescence signals and have good photothermal and photodynamic effects. Meanwhile, the loaded anticancer drug DOX was effectively released due to the photothermal effect of DPP-BT triggered the melting of the PCM. After intravenous injection of P(DPP-BT/DOX) NPs into Hela-bearing mice, NIR-II fluorescence/PA dual-modality imaging can be used to accurately monitor the size and specific location of the tumor during the treatment process in real-time (Fig. 9B and C). In general, simply co-encapsulating PSs, PATs, drugs and PCMs within a single nanoplatform can achieve precise combined

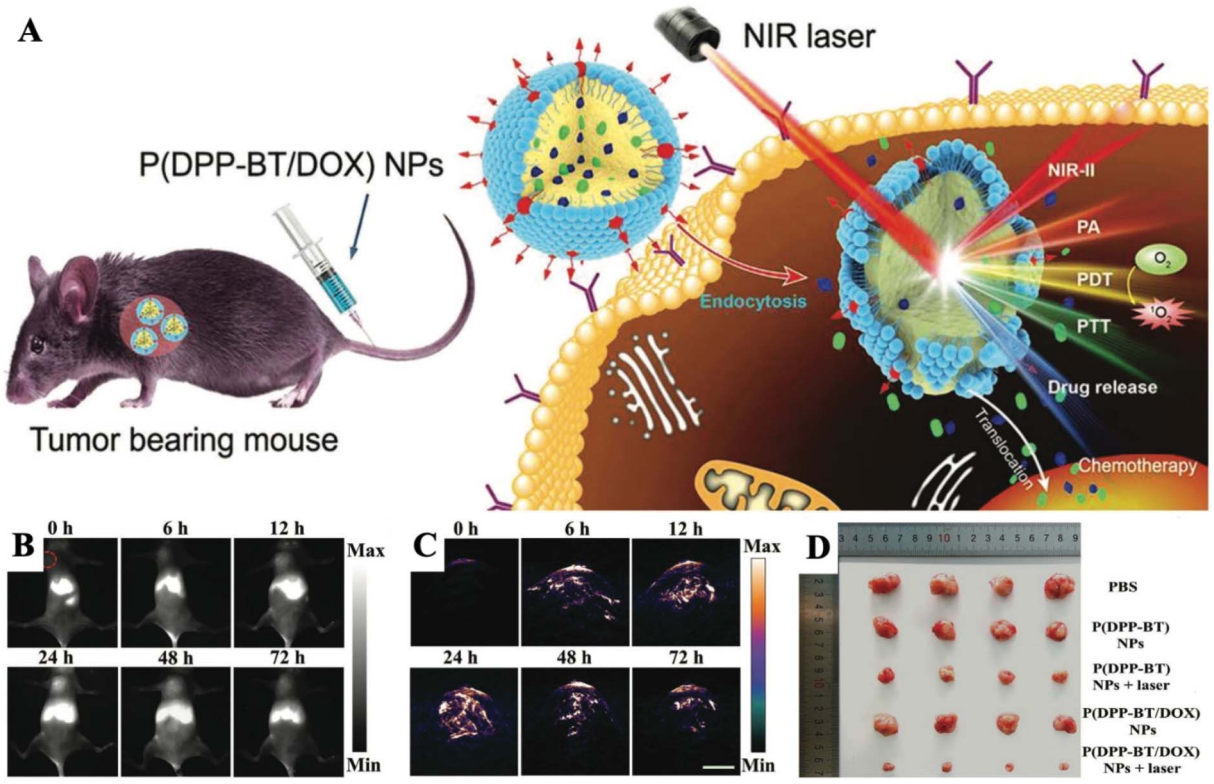

Fig. 9 (A) Schematic illustration of NIR laser-triggered, NIR-II fluorescence/PA dual-modality imaging-guided, tumor-targeted PTT/PDT/Chemo combination therapy. (B) NIR-II fluorescence imaging of tumor-bearing mice after injection of P(DPP-BT/DOX) NPs. (C) PA imaging of tumor-bearing mice after injection of P(DPP-BT/DOX) NPs. Scale bar: 3.5 mm. (D) Images of mice from different groups after 14 days of treatment. Adapted with permission from ref. 80. Copyright 2019 Wiley-VCH.

Open Access Article. Published on 13 November 2020. Downloaded on 12/5/2025 12:37:40 AM.
This article is licensed under a Creative Commons Attribution-NonCommercial 3.0 Unported Licence.

therapy in real-time monitoring of multimodal imaging. Due to the powerful light-mediated controlled release and seal protection capabilities of PCMs, the current stage of diagnosis and treatment technology has been successfully integrated into a nanoplatform, and it is versatile, which reduces the difficulty for clinical applications.

5. PCM-based nanoplatforms for PTT/CDT/Chemo combination therapy

CDT is another emerging cancer therapy that converts H_2O_2 into cytotoxic $^{\bullet}OH$ by Fenton or Fenton-like reactions at tumor sites.[81–83] Recently, various catalysts for CDT have been developed, such as Fe^{2+}, Fe^{3+}, Mn^{2+}, Cu^{+}, Cu^{2+}, V^{2+}, and Cr^{4+}.[84–89] CDT has shown noteworthy advantages in overcoming the hindrances of hypoxic TMEs and the limited laser penetration depth.[90] However, due to the limitation of H_2O_2 generated endogenously, the efficiency of CDT is still limited.[91,92] In this case, increasing the concentration of endogenous H_2O_2 or improving the catalytic ability of Fenton agents shows great promise for improving the CDT efficiency. Therefore, there is an urgent need to design a safer and much more efficient nanocarrier that can safely control H_2O_2 production in order to improve the efficiency of CDT.[93,94] Herein, our group adjusted a PCM with a melting point of 46 °C to co-wrap ultra-small CaO_2 NPs and iron-gallic acid (Fe-GA) NPs (Fenton agent with the photothermal effect) to prepare the final Fe-GA/CaO_2@PCM NPs for enhanced CDT (Fig. 10A).[95] Owing to the protection of the PCM, CaO_2 can avoid contact with the external environment, thereby reducing the premature release of CaO_2 and enhancing its stability. When under NIR laser irradiation, the high temperature produced by Fe-GA caused the PCM to melt, resulting in the burst release of CaO_2 NPs. The acidic TME then further activated CaO_2 NPs to generate large amounts of H_2O_2 and Ca^{2+}, thereby realizing high efficacy in Fe-GA-based CDT and Ca^{2+} induced cancer cell apoptosis, respectively. At the

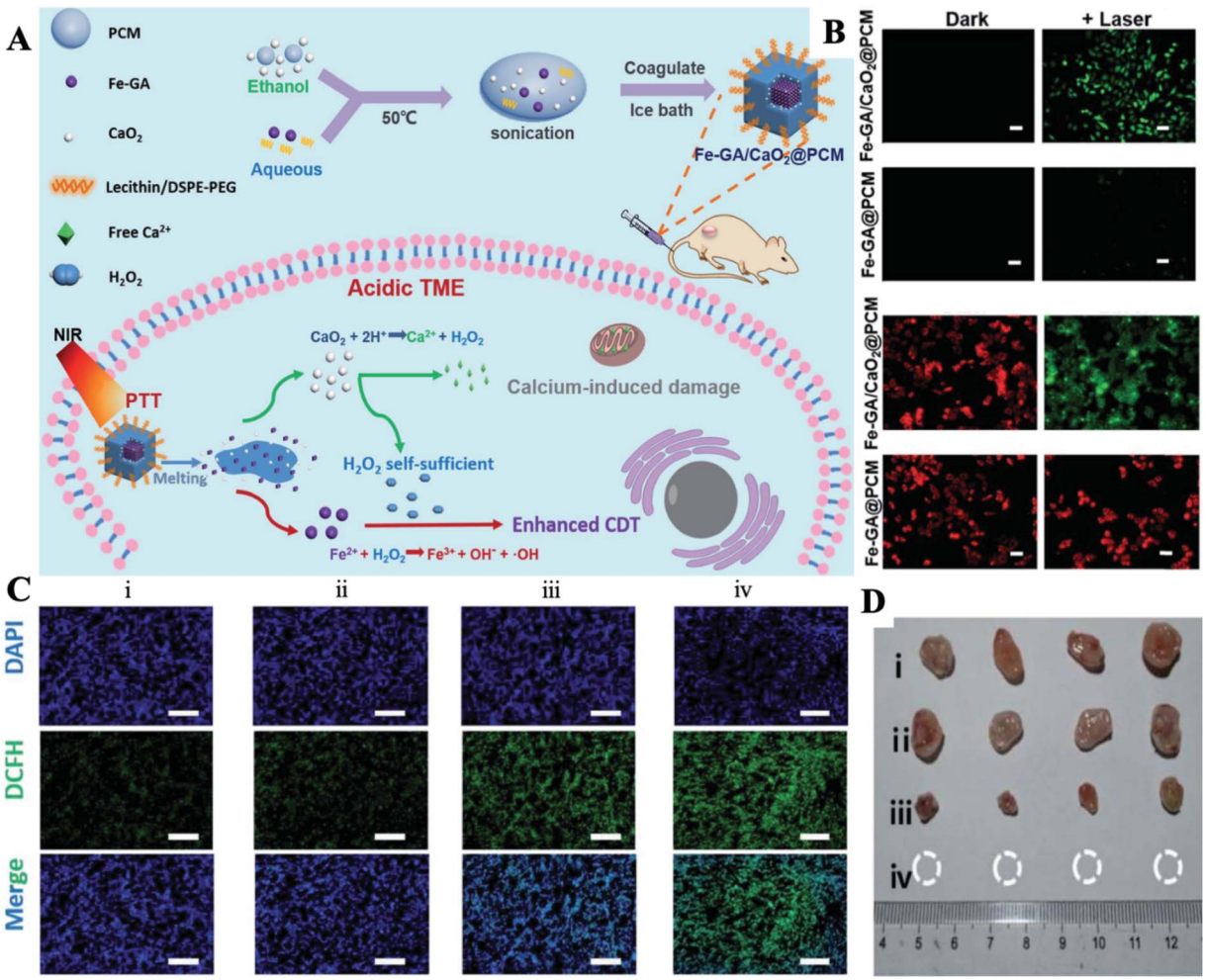

Fig. 10 (A) Schematic diagram of the preparation of the Fe-GA/CaO_2@PCM and its application in H_2O_2 self-sufficient PTT/CDT/Chemo combination therapy. (B) The detection of intracellular $^{\bullet}OH$ using the DCFH-DA probe and the staining of the mitochondrial membrane using the JC-1 probe. (C) The detection of intratumoral $^{\bullet}OH$ after different treatments using immunofluorescence staining of DCFH-DA. (D) Tumor volume curves for different treatment groups. (i) Control; (ii) Fe-GA/CaO_2-PCM; (iii) Fe-GA-PCM + laser; (iv) Fe-GA/CaO_2-PCM + laser. Adapted with permission from ref. 95. Copyright 2020 The Royal Society of Chemistry.

© 2021 The Author(s). Published by the Royal Society of Chemistry

Open Access Article. Published on 13 November 2020. Downloaded on 12/5/2025 12:37:40 AM.
This article is licensed under a Creative Commons Attribution-NonCommercial 3.0 Unported Licence.

same time, the hyperthermia produced by Fe-GA can not only effectively induce the death of cancer cells, but also accelerate the generation of ˙OH with the guidance of PAI and fluorescence imaging (Fig. 10B and C). By using H_2O_2 self-sufficient Fe-GA/CaO_2@PCM NPs, PTT/CDT/Chemo combination therapy showed excellent performance in inhibiting tumor growth (Fig. 10D). Due to their good biocompatibility and thermal response, Fe-GA/CaO_2@PCM NPs may become a potential multifunctional nanoplatform, which can provide self-supplied H_2O_2 to enhance PTT/CDT/Chemo processing on demand.

6. PCM-based nanoplatforms for SDT

SDT uses acoustic sensitizers to produce ROS to induce cell damage using ultrasound (US).[96,97] The competitive advantage of this treatment is that it is non-invasive and has a high tissue penetration depth. Similar to that of PDT, the therapeutic effect of SDT is also closely related to the oxygen supply conditions of tumor sites. In addition, previous studies have confirmed that the upregulated GSH levels in tumors would lead to an ineffective tumor suppression effect.[98,99] Therefore, there is an urgent need to systematically regulate TMEs while increasing the local oxygen concentration and inhibiting GSH levels.[100–103] Hao *et al.* covalently anchored the organic acoustic sensitizer protoporphyrin IX (PpIX) to biocompatible and biodegradable hollow mesoporous organic silica NPs (HMON).[104] K_2FeO_4, an oxygen producer, was then loaded into the surface mesopores of HMON–PpIX. Considering the extreme reactivity of K_2FeO_4 with water, PCMs made using lauric acid were used to insulate NPs from water for preparing the final Fe(VI)/PpIX-PCM@HMON (FHPLP) NPs. The high temperature caused by the US radiation will trigger the phase change of the PCM, thereby realizing US-responsive oxygen generation and ROS release. The final treatment efficiency was attributed to the *in situ* tumor reoxygenation, increased ROS generation and the glutathione depletion (Fig. 11A–C). *In vivo* experiments showed that the temperature could increase to 50.8 °C under the action of ultrasound, which is sufficient for the hyperthermia effect on the tumor. Furthermore, FHPLP with the US group obtained the highest PAI intensity and has excellent monitoring capabilities for tumor sites. The comparison of the regenerated oxygen concentration before and after the injection showed that the FHPLP also has a good improvement in tumor oxygenation. The *in vivo* therapeutic effect for tumor-bearing mice for 15 days showed that the combination therapy of FHPLP has a good inhibitory effect on tumor growth (Fig. 11D). All this showed that PCM-based SDT treatment nanoplatforms have broad application prospects.

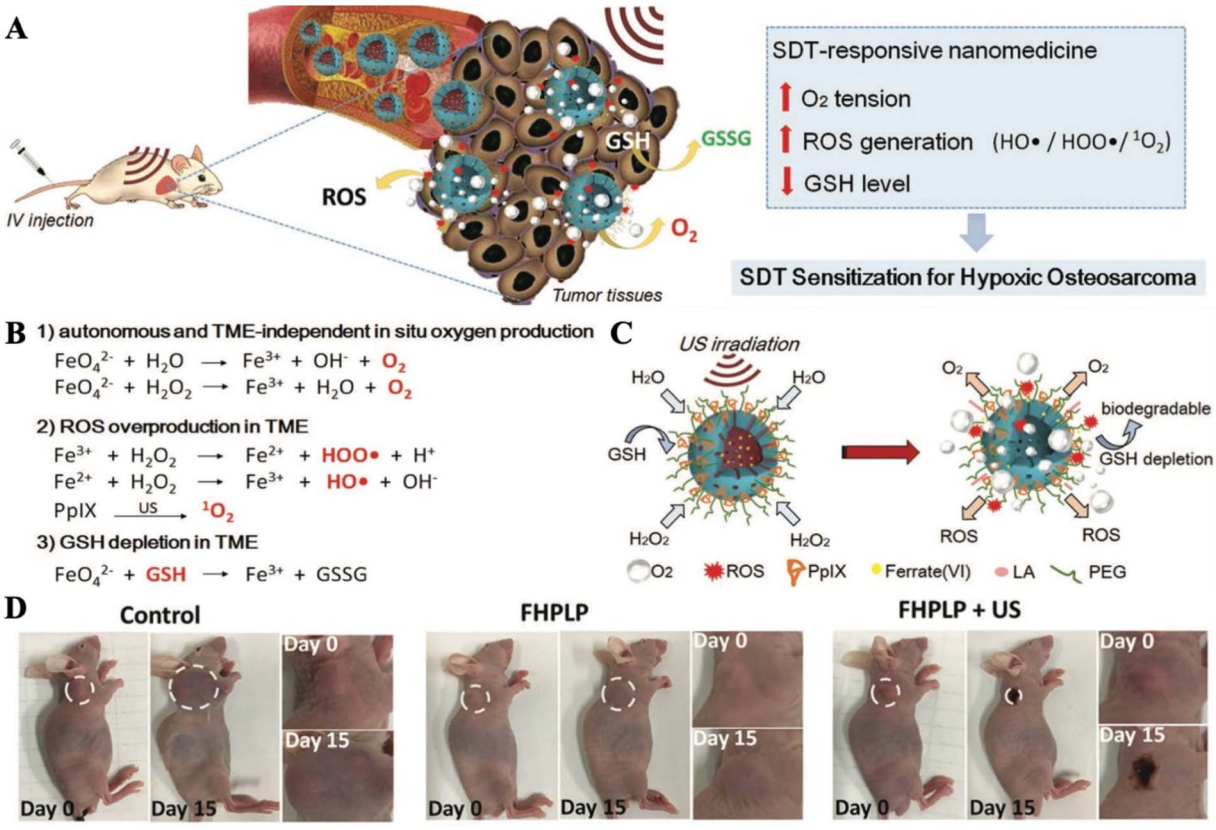

Fig. 11 (A) Schematic diagram of Fe(VI)/PpIX-PCM@HMON SDT-responsive production of oxygen, ROS generation and GSH consumption. (B) The specific mechanism of the production of oxygen, the generation of ROS and the consumption of GSH. (C) Schematic illustration of the synergistic and sensitized SDT with Fe(VI)/PpIX-PCM@HMON. (D) Photographs of mice bearing Saos-2 tumors on days 0 and 15 in different groups. Adapted with permission from ref. 104. Copyright 2019 Wiley-VCH.

© 2021 The Author(s). Published by the Royal Society of Chemistry

Open Access Article. Published on 13 November 2020. Downloaded on 12/5/2025 12:37:40 AM.
This article is licensed under a Creative Commons Attribution-NonCommercial 3.0 Unported Licence.

7. Summary and outlook

In this review, the recent progress in developing different kinds of PCM-based nanoplatforms for cancer therapy has been discussed. PCMs, mainly formulated with a certain proportion of natural fatty acids and their derivatives, show great advantages such as natural biocompatibility and biodegradability, large loading capacity, a stable and adjustable melting point, high abundance, diversity and low cost. The wax-seal feature of PCMs makes them excellent gatekeepers, thus making payloads stable in the circulation and preventing payloads such as anticancer drugs, ions, reactive species and even nanoparticles (MnO_2 and CaO_2) from premature release. Meanwhile, the thermo-responsive solid-to-liquid transition of PCMs enables the controlled release of payloads, which effectively reduce the side effects and enhance the therapeutic efficiency. Owing to the easy manufacturing process and versatile integration with other functional materials, PCM-based nanoplatforms exhibit great potential in cancer treatments.

Although PCM-based nanoplatforms have achieved great success in cancer therapy especially combined cancer treatments, there are still some challenges that need more attention in the future. Firstly, recently developed PCM-based nanoplatforms for cancer therapy are always triggered by the NIR laser irradiation induced thermal effect. The tissue penetration of NIR laser irradiation especially the NIR-I laser is always limited, thus influencing the therapeutic efficiency. Utilizing other methods such as high intensity focused ultrasound and a magnetic field to control the release of payloads at tumor sites might be more effect and sensitive. Secondly, until now, few studies have mixed PCMs with different melting points into a single nanoplatform. One direction for future development of PCM-based nanoplatforms is to load different types of drugs into PCMs to realize early release of payloads encapsulated in low melting point PCMs and later release of payloads encapsulated in high melting point PCMs, which is similar to a cocktail of therapies that can greatly reduce the severe drug resistance produced by a single administration. Thirdly, even with the support of PCMs, the specific identification and targeting of tumors remain unsolved. In the future, the composition of PCMs may be reconstructed for realizing the multiple functionalities of PCMs on the basis of TME biomarkers. Finally, although *in vivo* toxicity testing of PCM-based nanoplatforms has been performed in a mouse subcutaneous tumor model, to be clinically feasible, increased efforts should be made in the future to evaluate the responsiveness, stability, cycling, biodistribution, pharmacokinetics, degradability, and biological clearance mechanism of PCM-based NPs in the complex physiological environment of animals.

We hope that this paper would not only assist researchers in understanding the strategy of PCM-based nanoplatforms for combination cancer therapy, but also provide some ideas for designing smarter and more versatile PCM-based nanoplatforms for the treatment of cancer and other life-threatening diseases.

Conflicts of interest

There are no conflicts to declare.

Acknowledgements

The work was supported by the NNSF of China (61935004, 61525402, and 61775095), Jiangsu Provincial Key Research and Development Plan (BE2017741), Jiangsu Province Policy Guidance Plan (BZ2019014), and the Natural Science Foundation of Jiangsu Province (BK2018077).

References

1 Y. Cai, Z. Wei, C. Song, C. Tang, W. Han and X. Dong, *Chem. Soc. Rev.*, 2019, **48**, 22–37.
2 N. Yang, W. Xiao, X. Song, W. Wang and X. Dong, *Nano-Micro Lett.*, 2020, **12**, 15.
3 X. Huang, W. Zhang, G. Guan, G. Song, R. Zou and J. Hu, *Acc. Chem. Res.*, 2017, **50**, 2529–2538.
4 P. C. Lo, M. S. Rodriguez-Morgade, R. K. Pandey, D. K. P. Ng, T. Torres and F. Dumoulin, *Chem. Soc. Rev.*, 2020, **49**, 1041–1056.
5 H. Lin, Y. Chen and J. Shi, *Chem. Soc. Rev.*, 2018, **47**, 1938–1958.
6 N. Rabiee, M. T. Yaraki, S. M. Garakani, S. M. Garakani, S. Ahmadi, A. Lajevardi, M. Bagherzadeh, M. Rabiee, L. Tayebi, M. Tahriri and M. R. Hamblin, *Biomaterials*, 2020, **232**, 119707.
7 A. Fallahi, G. Guldentops, M. J. Tao, S. Granados-Focil and S. Van Dessel, *Appl. Therm. Eng.*, 2017, **127**, 1427–1441.
8 Y. Zhang, M. M. Umair, S. F. Zhang and B. T. Tang, *J. Mater. Chem. A*, 2019, **7**, 22218–22228.
9 J. Qiu, D. Huo and Y. Xia, *Adv. Mater.*, 2020, **32**, e2000660.
10 C. Cao, W. Ge, J. Yin, D. Yang, W. Wang, X. Song, Y. Hu, J. Yin and X. Dong, *Small*, 2020, **16**, e2000436.
11 J. Zhang, H. Huang, L. Xue, L. Zhong, W. Ge, X. Song, Y. Zhao, W. Wang and X. Dong, *Biomaterials*, 2020, **256**, 120211.
12 Z. Zhang, J. Wang, X. Nie, T. Wen, Y. Ji, X. Wu, Y. Zhao and C. Chen, *J. Am. Chem. Soc.*, 2014, **136**, 7317–7326.
13 D. C. Hyun, N. S. Levinson, U. Jeong and Y. Xia, *Angew. Chem., Int. Ed.*, 2014, **53**, 3780–3795.
14 P. Liang, X. Huang, Y. Wang, D. Chen, C. Ou, Q. Zhang, J. Shao, W. Huang and X. Dong, *ACS Nano*, 2018, **12**, 11446–11457.
15 C. Zhu, D. Huo, Q. Chen, J. Xue, S. Shen and Y. Xia, *Adv. Mater.*, 2017, **29**, 1703702.
16 B. Shi, N. Ren, L. Gu, G. Xu, R. Wang, T. Zhu, Y. Zhu, C. Fan, C. Zhao and H. Tian, *Angew. Chem., Int. Ed.*, 2019, **58**, 16826–16830.
17 R. Wang, K. Dong, G. Xu, B. Shi, T. Zhu, P. Shi, Z. Guo, W. H. Zhu and C. Zhao, *Chem. Sci.*, 2019, **10**, 2785–2790.
18 X. W. Lou, L. A. Archer and Z. C. Yang, *Adv. Mater.*, 2008, **20**, 3987–4019.
19 Z. Z. Li, L. X. Wen, L. Shao and J. F. Chen, *J. Controlled Release*, 2004, **98**, 245–254.

© 2021 The Author(s). Published by the Royal Society of Chemistry

Open Access Article. Published on 13 November 2020. Downloaded on 12/5/2025 12:37:40 AM.
This article is licensed under a Creative Commons Attribution-NonCommercial 3.0 Unported Licence.

20 M. S. Yavuz, Y. Cheng, J. Chen, C. M. Cobley, Q. Zhang, M. Rycenga, J. Xie, C. Kim, K. H. Song, A. G. Schwartz, L. V. Wang and Y. Xia, *Nat. Mater.*, 2009, **8**, 935–939.
21 G. D. Moon, S. W. Choi, X. Cai, W. Li, E. C. Cho, U. Jeong, L. V. Wang and Y. Xia, *J. Am. Chem. Soc.*, 2011, **133**, 4762–4765.
22 H. Cheng, D. Huo, C. Zhu, S. Shen, W. Wang, H. Li, Z. Zhu and Y. Xia, *Biomaterials*, 2018, **178**, 517–526.
23 S. Shen, C. Zhu, D. Huo, M. Yang, J. Xue and Y. Xia, *Angew. Chem., Int. Ed.*, 2017, **56**, 8801–8804.
24 Q. Chen, D. Huo, H. Cheng, Z. Lyu, C. Zhu, B. Guan and Y. Xia, *Adv. Healthcare Mater.*, 2019, **8**, e1801113.
25 D. J. Martin, K. Qiu, S. A. Shevlin, A. D. Handoko, X. Chen, Z. Guo and J. Tang, *Angew. Chem., Int. Ed.*, 2014, **53**, 9240–9245.
26 Y. Hui, X. Yi, F. Hou, D. Wibowo, F. Zhang, D. Zhao, H. Gao and C. X. Zhao, *ACS Nano*, 2019, **13**, 7410–7424.
27 X. Qian, X. Han and Y. Chen, *Biomaterials*, 2017, **142**, 13–30.
28 J. L. Perry, K. G. Reuter, J. C. Luft, C. V. Pecot, W. Zamboni and J. M. DeSimone, *Nano Lett.*, 2017, **17**, 2879–2886.
29 S. Dong, Y. N. Zhang, J. Wan, R. Cui, X. Yu, G. Zhao and K. Lin, *J. Mater. Chem. B*, 2020, **8**, 368–379.
30 E. A. Sykes, J. Chen, G. Zheng and W. C. Chan, *ACS Nano*, 2014, **8**, 5696–5706.
31 Y. Xia, W. Li, C. M. Cobley, J. Chen, X. Xia, Q. Zhang, M. Yang, E. C. Cho and P. K. Brown, *Acc. Chem. Res.*, 2011, **44**, 914–924.
32 X. Yang, M. Yang, B. Pang, M. Vara and Y. Xia, *Chem. Rev.*, 2015, **115**, 10410–10488.
33 X. Zhang, K. Wang, M. Liu, X. Zhang, L. Tao, Y. Chen and Y. Wei, *Nanoscale*, 2015, **7**, 11486–11508.
34 M. Liu, G. Zeng, K. Wang, Q. Wan, L. Tao, X. Zhang and Y. Wei, *Nanoscale*, 2016, **8**, 16819–16840.
35 A. Hussain and S. Guo, *J. Mater. Chem. B*, 2019, **7**, 974–985.
36 X. J. Song, Q. Chen and Z. Liu, *Nano Res.*, 2015, **8**, 340–354.
37 D. Xiao, J. J. Hu, J. Y. Zhu, S. B. Wang, R. X. Zhuo and X. Z. Zhang, *Nanoscale*, 2016, **8**, 16702–16709.
38 X. Wang, J. Feng, Y. Bai, Q. Zhang and Y. Yin, *Chem. Rev.*, 2016, **116**, 10983–11060.
39 J. Li, F. Zhang, Z. Hu, W. Song, G. Li, G. Liang, J. Zhou, K. Li, Y. Cao, Z. Luo and K. Cai, *Adv. Healthcare Mater.*, 2017, **6**, 1700005.
40 X. Duan, J. Xiao, Q. Yin, Z. Zhang, H. Yu, S. Mao and Y. Li, *ACS Nano*, 2013, **7**, 5858–5869.
41 J. Lehar, A. S. Krueger, W. Avery, A. M. Heilbut, L. M. Johansen, E. R. Price, R. J. Rickles, G. F. Short 3rd, J. E. Staunton, X. Jin, M. S. Lee, G. R. Zimmermann and A. A. Borisy, *Nat. Biotechnol.*, 2009, **27**, 659–666.
42 H. Chen, Y. Ma, X. Wang and Z. Zha, *J. Mater. Chem. B*, 2017, **5**, 7051–7058.
43 P. Yang, S. Gai and J. Lin, *Chem. Soc. Rev.*, 2012, **41**, 3679–3698.
44 X. Liu, J. Zhou, T. Yu, C. Chen, Q. Cheng, K. Sengupta, Y. Huang, H. Li, C. Liu, Y. Wang, P. Posocco, M. Wang, Q. Cui, S. Giorgio, M. Fermeglia, F. Qu, S. Pricl, Y. Shi, Z. Liang, P. Rocchi, J. J. Rossi and L. Peng, *Angew. Chem., Int. Ed.*, 2014, **53**, 11822–11827.
45 F. Tang, L. Li and D. Chen, *Adv. Mater.*, 2012, **24**, 1504–1534.
46 S.-H. Seo, B.-M. Kim, A. Joe, H.-W. Han, X. Chen, Z. Cheng and E.-S. Jang, *Biomaterials*, 2014, **35**, 3309–3318.
47 L. Tang and J. Cheng, *Nano Today*, 2013, **8**, 290–312.
48 J. Qiu, D. Huo, J. Xue, G. Zhu, H. Liu and Y. Xia, *Angew. Chem., Int. Ed.*, 2019, **58**, 10606–10611.
49 J. Della Rocca, D. Liu and W. Lin, *Acc. Chem. Res.*, 2011, **44**, 957–968.
50 H. Zhang, H. Wang, S. T. Williams, D. Xiong, W. Zhang, C. C. Chueh, W. Chen and A. K. Jen, *Adv. Mater.*, 2017, **29**, 1606608.
51 H. C. Zhou, J. R. Long and O. M. Yaghi, *Chem. Rev.*, 2012, **112**, 673–674.
52 P. Horcajada, R. Gref, T. Baati, P. K. Allan, G. Maurin, P. Couvreur, G. Ferey, R. E. Morris and C. Serre, *Chem. Rev.*, 2012, **112**, 1232–1268.
53 C. He, D. Liu and W. Lin, *Chem. Rev.*, 2015, **115**, 11079–11108.
54 R. C. Huxford, J. Della Rocca and W. Lin, *Curr. Opin. Chem. Biol.*, 2010, **14**, 262–268.
55 S. Nagata, K. Kokado and K. Sada, *Chem. Commun.*, 2015, **51**, 8614–8617.
56 C. Y. Sun, C. Qin, X. L. Wang, G. S. Yang, K. Z. Shao, Y. Q. Lan, Z. M. Su, P. Huang, C. G. Wang and E. B. Wang, *Dalton Trans.*, 2012, **41**, 6906–6909.
57 J. F. Yao, Y. Huang and H. T. Wang, *J. Mater. Chem.*, 2010, **20**, 9827–9831.
58 Q. Wu, M. Niu, X. Chen, L. Tan, C. Fu, X. Ren, J. Ren, L. Li, K. Xu, H. Zhong and X. Meng, *Biomaterials*, 2018, **162**, 132–143.
59 D. Chen, Z. Zhong, Q. Ma, J. Shao, W. Huang and X. Dong, *ACS Appl. Mater. Interfaces*, 2020, **12**, 26914–26925.
60 Y. Wang, J. Zhang, X. Lv, L. Wang, Z. Zhong, D. P. Yang, W. Si, T. Zhang and X. Dong, *Biomaterials*, 2020, **252**, 120111.
61 G. Liu, J. Zhu, H. Guo, A. Sun, P. Chen, L. Xi, W. Huang, X. Song and X. Dong, *Angew. Chem., Int. Ed.*, 2019, **58**, 18641–18646.
62 T. K. Ryu, S. W. Baek, R. H. Kang, K. Y. Jeong, D. R. Jun and S. W. Choi, *J. Controlled Release*, 2018, **270**, 237–245.
63 G. Liu, S. Zhang, Y. Shi, X. Huang, Y. Tang, P. Chen, W. Si, W. Huang and X. Dong, *Adv. Funct. Mater.*, 2018, **28**, 1804317.
64 X. Dang, J. Scotcher, S. Wu, R. K. Chu, N. Tolic, I. Ntai, P. M. Thomas, R. T. Fellers, B. P. Early, Y. Zheng, K. R. Durbin, R. D. Leduc, J. J. Wolff, C. J. Thompson, J. Pan, J. Han, J. B. Shaw, J. P. Salisbury, M. Easterling, C. H. Borchers, J. S. Brodbelt, J. N. Agar, L. Pasa-Tolic, N. L. Kelleher and N. L. Young, *Proteomics*, 2014, **14**, 1130–1140.
65 X. Li, B. Y. Zheng, M. R. Ke, Y. Zhang, J. D. Huang and J. Yoon, *Theranostics*, 2017, **7**, 2746–2756.
66 Q. Y. Tang, W. Y. Xiao, C. H. Huang, W. L. Si, J. J. Shao, W. Huang, P. Chen, Q. Zhang and X. C. Dong, *Chem. Mater.*, 2017, **29**, 5216–5224.

© 2021 The Author(s). Published by the Royal Society of Chemistry

Open Access Article. Published on 13 November 2020. Downloaded on 12/5/2025 12:37:40 AM.
This article is licensed under a Creative Commons Attribution-NonCommercial 3.0 Unported Licence.

67 G. Liu, J. Zou, Q. Tang, X. Yang, Y. Zhang, Q. Zhang, W. Huang, P. Chen, J. Shao and X. Dong, *ACS Appl. Mater. Interfaces*, 2017, **9**, 40077–40086.
68 T. Wang, D. Wang, H. Yu, M. Wang, J. Liu, B. Feng, F. Zhou, Q. Yin, Z. Zhang, Y. Huang and Y. Li, *ACS Nano*, 2016, **10**, 3496–3508.
69 L. Shen, Z. Chen, Y. Li, S. He, S. Xie, X. Xu, Z. Liang, X. Meng, Q. Li, Z. Zhu, M. Li, X. C. Le and Y. Shao, *Anal. Chem.*, 2008, **80**, 6323–6328.
70 G. Ramirez-Garcia, M. Martinez-Alfaro, F. d'Orlye, F. Bedioui, N. Mignet, A. Varenne, S. Gutierrez-Granados and C. Richard, *Int. J. Pharm.*, 2017, **532**, 696–703.
71 Y. Y. Li, G. Wang, X. G. Zhu, M. H. Liu, C. Ye, X. Chen, Y. Y. Wang, K. He, L. L. Wang, X. C. Ma, H. J. Zhang, X. Dai, Z. Fang, X. C. Xie, Y. Liu, X. L. Qi, J. F. Jia, S. C. Zhang and Q. K. Xue, *Adv. Mater.*, 2010, **22**, 4002–4007.
72 J. Zou, J. Zhu, Z. Yang, L. Li, W. Fan, L. He, W. Tang, L. Deng, J. Mu, Y. Ma, Y. Cheng, W. Huang, X. Dong and X. Chen, *Angew. Chem., Int. Ed.*, 2020, **59**, 8833–8838.
73 Y. Wang, X. Huang, Y. Tang, J. Zou, P. Wang, Y. Zhang, W. Si, W. Huang and X. Dong, *Chem. Sci.*, 2018, **9**, 8103–8109.
74 G. Yang, L. Xu, Y. Chao, J. Xu, X. Sun, Y. Wu, R. Peng and Z. Liu, *Nat. Commun.*, 2017, **8**, 902.
75 S. C. Zhang, Q. Z. Li, N. Yang, Y. H. Shi, W. Ge, W. J. Wang, W. Huang, X. J. Song and X. C. Dong, *Adv. Funct. Mater.*, 2019, **29**, 1906805.
76 C. Liang, X. Zhang, M. Yang and X. Dong, *Adv. Mater.*, 2019, **31**, e1904197.
77 C. Liang, X. Zhang, M. Yang, W. Wang, P. Chen and X. Dong, *ACS Mater. Lett.*, 2020, 1268–1286, DOI: 10.1021/acsmaterialslett.0c00259.
78 Y. Dai, J. Su, K. Wu, W. Ma, B. Wang, M. Li, P. Sun, Q. Shen, Q. Wang and Q. Fan, *ACS Appl. Mater. Interfaces*, 2019, **11**, 10540–10553.
79 D. Chen, Y. Tang, J. Zhu, J. Zhang, X. Song, W. Wang, J. Shao, W. Huang, P. Chen and X. Dong, *Biomaterials*, 2019, **221**, 119422.
80 Q. Wang, Y. Dai, J. Xu, J. Cai, X. Niu, L. Zhang, R. Chen, Q. Shen, W. Huang and Q. Fan, *Adv. Funct. Mater.*, 2019, **29**, 1616–3028.
81 M. Huo, L. Wang, Y. Chen and J. Shi, *Nat. Commun.*, 2017, **8**, 357.
82 L. H. Fu, Y. R. Hu, C. Qi, T. He, S. Jiang, C. Jiang, J. He, J. Qu, J. Lin and P. Huang, *ACS Nano*, 2019, **13**, 13985–13994.
83 Z. Tang, Y. Liu, M. He and W. Bu, *Angew. Chem., Int. Ed.*, 2019, **58**, 946–956.
84 Z. Yang, Y. Dai, L. Shan, Z. Shen, Z. Wang, B. C. Yung, O. Jacobson, Y. Liu, W. Tang, S. Wang, L. Lin, G. Niu, P. Huang and X. Chen, *Nanoscale Horiz.*, 2019, **4**, 426–433.
85 Z. Zhou, J. Song, R. Tian, Z. Yang, G. Yu, L. Lin, G. Zhang, W. Fan, F. Zhang, G. Niu, L. Nie and X. Chen, *Angew. Chem., Int. Ed.*, 2017, **56**, 6492–6496.
86 L. Zhang, S. S. Wan, C. X. Li, L. Xu, H. Cheng and X. Z. Zhang, *Nano Lett.*, 2018, **18**, 7609–7618.
87 P. Ma, H. Xiao, C. Yu, J. Liu, Z. Cheng, H. Song, X. Zhang, C. Li, J. Wang, Z. Gu and J. Lin, *Nano Lett.*, 2017, **17**, 928–937.
88 L. S. Lin, T. Huang, J. Song, X. Y. Ou, Z. Wang, H. Deng, R. Tian, Y. Liu, J. F. Wang, Y. Liu, G. Yu, Z. Zhou, S. Wang, G. Niu, H. H. Yang and X. Chen, *J. Am. Chem. Soc.*, 2019, **141**, 9937–9945.
89 H. Hou, X. Huang, G. Wei, F. Xu, Y. Wang and S. Zhou, *ACS Appl. Mater. Interfaces*, 2019, **11**, 29579–29592.
90 H. Ranji-Burachaloo, A. Reyhani, P. A. Gurr, D. E. Dunstan and G. G. Qiao, *Nanoscale*, 2019, **11**, 5705–5716.
91 J. Y. Zhu, C. X. Li, P. Z. Chen, Z. W. Ma, B. Zou, L. Y. Niu, G. L. Cui and Q. Z. Yang, *Mater. Chem. Front.*, 2020, **4**, 176–181.
92 D. Li, L. Chen, T. Wang and L. Z. Fan, *ACS Appl. Mater. Interfaces*, 2018, **10**, 7069–7078.
93 V. Biju, *Chem. Soc. Rev.*, 2014, **43**, 744–764.
94 N. Bertrand, J. Wu, X. Xu, N. Kamaly and O. C. Farokhzad, *Adv. Drug Delivery Rev.*, 2014, **66**, 2–25.
95 S. C. Zhang, C. Y. Cao, X. Y. Lv, H. M. Dai, Z. H. Zhong, C. Liang, W. J. Wang, W. Huang, X. J. Song and X. C. Dong, *Chem. Sci.*, 2020, **11**, 1926–1934.
96 W. Fan, P. Huang and X. Chen, *Chem. Soc. Rev.*, 2016, **45**, 6488–6519.
97 X. Qian, Y. Zheng and Y. Chen, *Adv. Mater.*, 2016, **28**, 8097–8129.
98 F. Gong, L. Cheng, N. Yang, O. Betzer, L. Feng, Q. Zhou, Y. Li, R. Chen, R. Popovtzer and Z. Liu, *Adv. Mater.*, 2019, **31**, e1900730.
99 I. S. Donskyi, Y. Chen, P. Nickl, G. Guday, H. Qiao, K. Achazi, A. Lippitz, W. E. S. Unger, C. Bottcher, W. Chen, M. Adeli and R. Haag, *Nanoscale*, 2020, **12**, 14222–14229.
100 Q. Chen, L. Feng, J. Liu, W. Zhu, Z. Dong, Y. Wu and Z. Liu, *Adv. Mater.*, 2016, **28**, 7129–7136.
101 P. Zhu, Y. Chen and J. Shi, *ACS Nano*, 2018, **12**, 3780–3795.
102 L. Feng, R. Xie, C. Wang, S. Gai, F. He, D. Yang, P. Yang and J. Lin, *ACS Nano*, 2018, **12**, 11000–11012.
103 L. Zhang, Z. Yang, J. H. Ren, L. Ba, W. S. He and C. Y. E. Wong, *Nano Res.*, 2020, **13**, 1389–1398.
104 J. Fu, T. Li, Y. Zhu and Y. Hao, *Adv. Funct. Mater.*, 2019, **29**, 1906195.

© 2021 The Author(s). Published by the Royal Society of Chemistry